CHAPTER

Membrane contactors

5

Patricia Luis
Materials & Process Engineering (iMMC-IMAP), Catholic University of Louvain, Louvain-la-Neuve, Belgium

CHAPTER OUTLINE

5.1 PROCESS DESCRIPTION

A membrane contactor is a device containing a ceramic or polymeric porous membrane in which the objective is to promote the contact between two phases. The membrane does not give selectivity to the separation since it is only a physical barrier that separates the two phases. Thus the kind of membrane considered in this Chapter relates to the *Approach ii* according to the classification indicated in Chapter 1. This involves that all compounds could permeate through the membrane without any selective separation. The selectivity of the separation is normally

Fundamental Modeling of Membrane Systems. https://doi.org/10.1016/B978-0-12-813483-2.00005-8

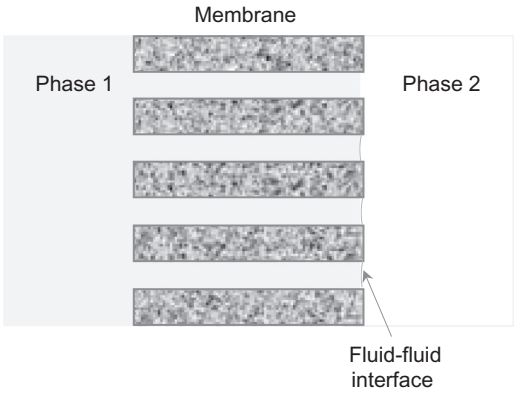

FIG. 5.1

General working principle of a membrane contactor.

obtained by using a separation fluid at the other side of the membrane. Thus the feed stream and the separation fluid will be in contact only through the membrane pores. A schematic diagram can be observed in Fig. 5.1. A membrane contactor is thus a device that achieves gas-liquid or liquid-liquid mass transfer without dispersion of one phase within another. This is accomplished by passing the fluids on opposite sides of a microporous membrane and controlling carefully the pressure difference between both fluids so that one of them is immobilized in the pores of the membrane and the fluid-fluid interface is located at the mouth of each pore. Gabelman and Hwang (1999) elaborated an inspiring review that has become a basic starting point for those that are interesting in this technology. The main role of the membrane is to act as a barrier and to increase the surface for mass transfer exchange between both phases. The main challenge of designing and operating conventional devices is to maximize the mass transfer rate by producing as much interfacial area as possible, and a major disadvantage is the interdependence of the two fluid phases to be contacted, which may lead to the formation of emulsions, foaming, unloading, and flooding. Thus nondispersive contact via a microporous membrane offered by the membrane contactor is a technological alternative to many conventional processes in the industry that overcomes those disadvantages while giving more interfacial area (Gabelman and Hwang, 1999). Table 5.1 presents several conventional processes that can be substituted by membrane contactors. Recognized advantages of using membrane contactors in comparison with a conventional process are more operational flexibility (independent control of fluid flow rates, no emulsions, no flooding at high flow rates, no unloading at low flow rates, no density difference between liquids required, no drop dragging of liquid phase), controlled and known high interfacial area, linear scale-up (modular equipment), compact, and less energy consuming. Membrane contactors typically offer 30 times more area than what is achievable in gas absorbers and 500 times what is obtainable in liquid-liquid extraction columns (Gabelman and Hwang, 1999).

Table 5.1 Conventional unit operations that can be substituted by membrane contactors

Conventional unit operations	Membrane contactors
Scrubbers/Strippers (absorption/desorption)	Membrane strippers/scrubbers
Packed columns, mixer-settler, centrifugal devices (liquid-liquid extraction)	Membrane extractors
Distillation columns, evaporators	Membrane distillation and osmotic distillation
Crystallizers	Membrane crystallizers
High pressure homogenizers	Membrane emulsifiers
Chemical reactors	Contactor membrane reactors

Several configurations are proposed when working with membrane contactors, such as flat sheets, capillary membranes, or hollow fiber membranes. However, hollow fiber membranes are the main applied configuration in current research due to the large contact surface that can provide. Sometimes, the membrane contactors found in the market are designed for pressure-driven filtration processes such as microfiltration or ultrafiltration, but they are proposed by researchers to fulfill other applications such as gas absorption or liquid-liquid extraction.

The mass transfer in membrane contactors takes place through the membrane pores thanks to a driving force generated by a difference of concentration (or partial pressure) and/or a difference of temperature. The kind of contacting phases (gas-liquid, liquid-liquid, liquid-solid) and the objective of the separation will determine the basic mechanisms of the driving force. Fig. 5.2 shows a summary of the different applications of membrane contactors as well as the phases involved, the profiles of driving forces, and the main kind of polarization that may occur (Drioli and Curcio, 2004; Curcio and Drioli, 2005).

Membrane distillation and osmotic membrane distillation use distillation process to remove water from a liquid stream in the form of vapor through the membrane pores. Microporous hydrophobic membranes are used, which will prevent membrane wetting, and volatile compounds of the feed solution may be transported through the membrane pores in gas phase due to a temperature and a concentration gradient (partial pressure difference) that acts as the driving force at both sides of the membrane, which depends on the temperature and composition in the layers adjacent to the membrane surface (Curcio and Drioli, 2005; Gryta, 2005). In the case of osmotic distillation, the transport of molecules through the membrane is due to a difference in vapor pressure provided by a low-vapor-pressure solution (normally a very concentrated osmotic solution) on the permeate side of the membrane. Thus the mass transfer will take place from the feed solution to the osmotic solution.

Membrane crystallization is an extension of membrane distillation with the objective of concentrating the salts present in the liquid stream until reaching supersaturation. Then, the concentrated liquid stream is passed through a crystallizer to

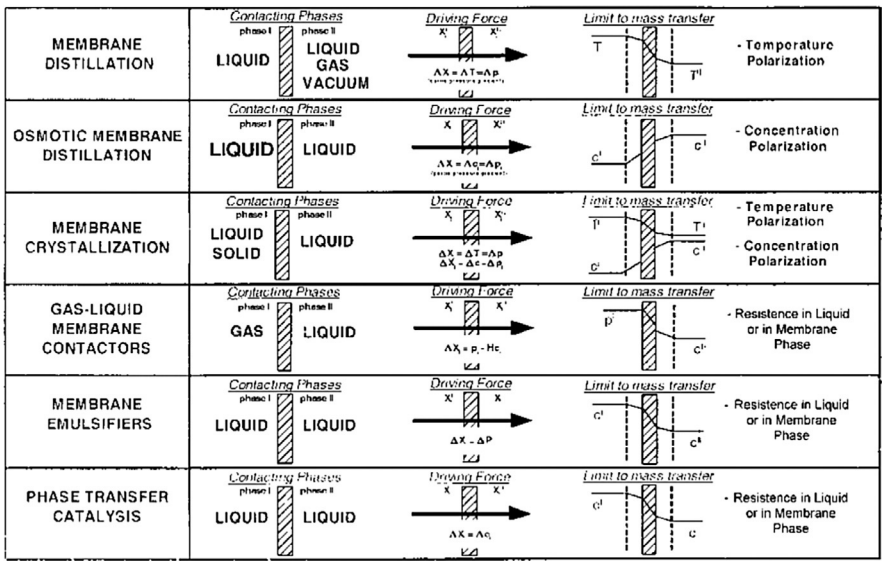

FIG. 5.2

Overview of membrane contactors.

Reprinted with permission from Curcio, E., Enrico, D., 2005. Membrane distillation and related operations—a review. Sep. Purif. Rev. 34, 35–86.

produce salt crystals. The presence of the membrane enhances heterogeneous nucleation, although crystals growing should take always place outside the contactor in order to prevent membrane blockage.

Gas-liquid membrane contactors allow the mass transfer from a gas phase stream to a liquid phase (e.g., absorption of CO_2, SO_2, NO, H_2S, NH_3, oxygen removal in semiconductor industry for the production of ultrapure water, carbonation of beverages, nitrogenation of beer to provide a dense foam head, ozonation for water treatment) or from a liquid stream to the gas phase (e.g., removal of trace of oxygen at levels of <10ppb from water for ultrapure water preparation for the electronics industry, the removal of CO_2 from fermentation broth) (Sengupta et al., 1998; Sirkar, 1995; Curcio and Drioli, 2005). The driving force is difference of concentrations or partial pressures at both sides of the membrane. The membrane pores are expected to be filled by gas so that the mass transfer resistance is lower, which will be determined by the transmembrane pressure.

Uniform emulsions can be produced by using membrane contactors since high-stable droplets are created by forcing the dispersed phase through the pores of the membrane, reducing energy input and wall shear stress with respect to high-pressure homogenizers and rotor-stator systems (Curcio and Drioli, 2005). In this case, the dispersed phase has to pass through the membrane pores to the dispersing phase. Thus considerations on how important is to avoid or at least minimize membrane

wetting, which are critical for the other systems based on membrane contactors, are not relevant in membrane emulsifiers. Membrane emulsification increases the stability of the emulsion and decreases coalescence phenomena. In addition, the droplet size can be easily controlled since it is directly related to the size of the membrane pores. Applications of membrane emulsification are mainly found in the preparation of food emulsions.

Finally, membrane contactors are also used to perform chemical reactions. Contactor membrane reactors are used to intensify the contact between reactants. The system may have a membrane which can be used as a barrier to separate two fluid phases, for example, two reactants or the reactants from an extracting agent, with the catalyst in solution or within the membrane pores (interfacial contactor); or it can work with the mixed reactants being pushed through the membrane pores, where the reaction will take place (forced flow-through contactor). The product will hence be collected at the other side of the membrane. A typical application of contactor membrane reactors is in phase transfer catalysis operations. The catalytically active phase deposited on the surface of inorganic membrane layers promotes the reaction between absorbed reactant species. A phase transfer catalyst is used to transfer a reactant from one phase into the other, allowing the reaction to occur (Drioli and Romano, 2001; Curcio and Drioli, 2005).

In membrane contactors, the membrane pores are typically filled by one of the two fluid phases. The fluid phase that will fill the membrane pores will be determined by the breakthrough pressure. The breakthrough pressure is the minimum pressure required for one phase to go through the membrane pores to the other side of the membrane. This pressure is calculated assuming that the pores are ideal cylinders (Charcosset et al., 2004):

$$P_c = \frac{4\gamma \cos\theta}{\overline{d_p}} \tag{5.1}$$

where P_c is the breakthrough pressure, γ the interfacial tension, θ the contact angle of the liquid to wet the membrane, and $\overline{d_p}$ the average pore diameter. If the transmembrane pressure is greater than the breakthrough pressure, the liquid will go through the membrane pores. Eq. (5.1) is not considering tortuosities in the pores, irregularities in the pore openings at the membrane surface, or effects of surface wettability. Thus the value predicted by Eq. (5.1) may be lower than the real one. The pressure difference has to be always lower than the breakthrough pressure unless the intention is to have the fluid going through the membrane as happens in membrane emulsification or in forced flow-through contactors. In membrane-based absorption, for example, membrane wetting is a nuisance and the gas phase is desired to be inside the pores of the membrane so that diffusion through the membrane pores is easier. Thus a good control of pressures is an important aspect in membrane contactors to ensure the stability of the phases in the system.

Membrane contactors are becoming a powerful technology with a large number of applications that includes gas-liquid, liquid-liquid, and liquid-liquid-solid systems. The main reason is the flexibility found in the kind of membranes that can

be used. The membrane acts merely as a barrier. No selectivity or separation is expected from the membrane, which means that only mechanical and chemical resistance is demanded. The driving force is achieved by using selective solvents, vacuum, sweep gas, osmotic solutions, and so on, depending on the system. Thus the membrane is never a limitation in terms of performance (although wetting and other operation issues may appear) and the researcher/user faces a tremendous freedom to develop new systems and applications. In the following subsections, specific aspects related to the general mathematical description of mass transfer in hollow fiber membrane contactors as well as specific aspects to consider in membrane-based absorption, membrane-based extraction, membrane distillation-crystallization, membrane emulsification, and contactor membrane reactors are presented.

5.2 MATHEMATICAL DESCRIPTION OF MASS TRANSFER IN A MEMBRANE CONTACTOR

The description of the mass transfer in a hollow fiber membrane contactor can be done by following different approaches. Assuming that the resistance to mass transfer is occurring only in films of fluid close to the membrane interface as well as in the membrane itself leads to a very simple model called the resistance-in-series model. Each resistance, that is, the resistances in the feed phase, the membrane, and the receptive phase, is represented by the inverse of a mass transfer coefficient, and the overall resistance by the inverse of an overall mass transfer coefficient. This model assumes linear profiles of concentration and thermodynamic equilibrium at the fluid-fluid interfaces within the membrane pores. More complex models can be developed if the concentration profiles are described by a differential mass balance in portion of fluids or even within the membrane. The following lines show a brief description of those possibilities.

5.2.1 FILM THEORY AND RESISTANCE-IN-SERIES MODEL

The film theory has been extensively applied to describe the mass transfer in systems in which fluid phases are present. The theory considers that the resistance to mass transfer in a given turbulent fluid phase is present in a thin layer adjacent to the interface that is called a film (Seader et al., 2011). In gas-liquid and liquid-liquid separation processes, the mass transfer resistance in both phases has to be considered, and the presence of a membrane introduces a third phase to be also evaluated. An example is shown in Fig. 5.3A for a gas-liquid interface where the component in fluid A diffuses into fluid B. If two films are considered (one for each fluid phase), one speaks about the double-film theory (Fig. 5.3B). When a porous membrane is present in between the two fluid phases, as happens in a membrane contactor, the same approach can be considered. In this case, the film is adjacent to the fluid-membrane interface, as represented in Fig. 5.3C.

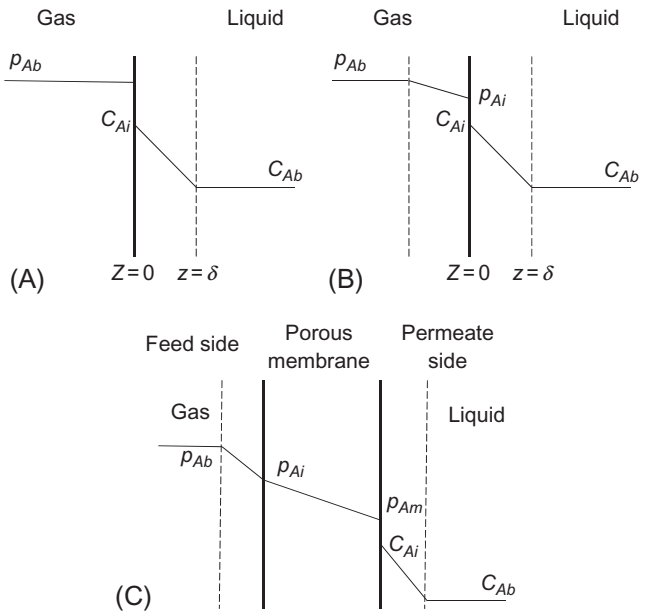

FIG. 5.3

Concentration and partial pressure profiles for solute transport through membranes: (A) film theory; (B) double-film theory; (C) double-film theory with a membrane in between the fluid phases.

At the interface, phase equilibrium is assumed. Thus a solubility relationship like Henry's law for gas-liquid systems ($H_A = c_A/p_A$), or a partition coefficient for liquid-liquid systems ($P = c_A/c_A'$), can be considered. Molecular diffusion occurs through the film of thickness δ with a driving force $c_{Ai} - c_{Ab}$, where c_{Ab} is the bulk average concentration of A in the receiving fluid phase in Fig. 5.3A. Thus applying and integrating the Fick's first law gives:

$$J_A = \frac{D_{AB}}{\delta}(c_{Ai} - c_{Ab}) = \frac{c \cdot D_{AB}}{\delta}(x_{Ai} - x_{Ab}) \tag{5.2}$$

If the film theory is extended to two films in series, each film presents a resistance to mass transfer but the concentrations in the two fluids at the interface are assumed to be in phase equilibrium. Considering steady-state mass transfer of A from a gas, across the gas-liquid interface, and into a liquid, the mass transfer can be written in the same way as Eq. (5.2). Normally, the ratio $\frac{D_{AB}}{\delta}$ is unknown since the thickness of the films depends on the flow conditions, and is replaced by a mass transfer coefficient for each film, which considers the mass transfer resistance of each film. This approach is the basis of the resistance-in-series model since each film of fluid and the membrane produces a specific resistance, represented by the inverse of the individual mass transfer coefficients. Thus

$$J_A = k_g(p_{Ab} - p_{Ai}) \tag{5.3a}$$

$$J_A = k_l(c_{Ai} - c_{Ab}) \tag{5.3b}$$

c_{Ai} and p_{Ai} are the concentration of the component A at the interface, in the liquid and gas side, respectively. They are related by the Henry's law since it is considered that they are in equilibrium: $c_{Ai} = H_A p_{Ai}$. Substituting the Henry's law relationship in Eq. (5.3b) to eliminate c_{Ai}, and introducing the resulting expression in Eq. (5.3a), gives:

$$J_A = \frac{p_{Ab}H_A - c_{Ab}}{(H_A/k_g) + (1/k_l)} \tag{5.4}$$

If a membrane is separating the two fluid phases as in Fig. 5.3C, Eqs. (5.3a), (5.3b) should be completed with a third equation that describes the mass transfer through the membrane (assuming gas in the pores):

$$J_A = k_m(p_{Ai} - p_{Am}) \tag{5.3c}$$

The equilibrium at the gas-liquid interface is given by $c_{Ai} = H_A p_{Am}$. Thus following the same substitution procedure, Eq. (5.4) would become:

$$J_A = \frac{p_{Ab}H_A - c_{Ab}}{(H_A/k_g) + (1/k_m) + (1/k_l)} \tag{5.5}$$

The overall mass transfer coefficient, $K_{overall}$, can be thus defined as

$$\frac{1}{K_{overall}} = \frac{H_A}{k_g} + \frac{1}{k_m} + \frac{1}{k_l} \tag{5.6}$$

Eq. (5.5) can be written as

$$J_A = K_{overall}(p_{Ab}H_A - c_{Ab}) \tag{5.7}$$

which is a very practical way to evaluate the mass transfer through the membrane since the bulk concentrations, p_{Ab} and c_{Ab}, are known. Eq. (5.6) is the basis of the resistance-in-series model. Each term of the equation represents one resistance to mass transfer, thus the overall resistance, $\frac{1}{K_{overall}}$, is the result of the sum of the resistances given by the gas phase (R_g), the membrane (R_m), and the liquid phase (R_l):

$$R_{overall} = R_g + R_m + R_l \tag{5.8}$$

The mathematical description shown previously is an example of mass transfer in a gas-liquid system with pores filled with gas. A more detailed explanation is included in the specific sections of this chapter.

5.2.2 MODELING BASED ON DIFFERENTIAL EQUATIONS

The mass transfer takes place through the membrane pores and no mixing between phases occurs. The fluid flow in the membrane contactor can be described using the laminar flow model in the tube side and the Happel's free surface model (Happel, 1959) in the shell side. The Happel's free surface model assumes that the fibers

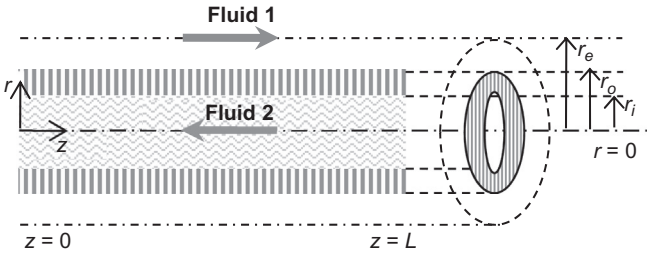

FIG. 5.4

Axial and radial coordinates of a fiber.

Reproduced with permission from Luis, P., Garea, A., Irabien, A., 2010. Modelling of a hollow fiber ceramic contactor for SO_2 absorption. Sep. Purif. Technol. 72, 174–179.

are distributed evenly through the shell space, which allows the results obtained with a single fiber to be generalized to the entire module (Gabelman and Hwang, 1999). The coordinates of a fiber are shown in Fig. 5.4. The radial position of $r=0$ is the center of a fiber and the radial distances r_i, r_o, and r_e are the inner radius, outer radius, and Happel's free distance of the fiber. The axial distance of $z=0$ means the inlet position of a fiber and the axial distance of $z=\mathrm{L}$ represents the outlet position of a fiber. One fluid phase is fed to the shell side at $z=0$ and the other fluid phase is passed through the tube side at $z=\mathrm{L}$. It is assumed that local equilibrium at the fluid-fluid interface takes place and mass transfer is only produced by diffusion.

Shell side

In order to describe the mass transfer in the shell side of the fiber, the following assumptions can be considered: (1) steady state and isothermal condition, (2) no axial diffusion, (3) using Happel's free surface model (Happel, 1959) to characterize the velocity profile at the shell side, (4) the physical properties of the fluid were constant, (5) constant shell side pressures. Based on the Happel's free surface model (Happel, 1959), only a portion of the fluid surrounding the fiber is considered, which may be approximated as a circular cross section.

The partial differential equation of the mass balance for cylindrical coordinates is obtained using Fick's law of diffusion and it is given as follows:

$$u_{z,g}\frac{\partial C_{A,feed}}{\partial z}=D_{A,feed}\left[\frac{1}{r}\frac{\partial}{\partial r}\left(r\frac{\partial C_{A,feed}}{\partial r}\right)\right] \tag{5.9}$$

The velocity profile in the shell side may be deduced from the Happel's free surface model (Happel, 1959):

$$u_{z,g}=u_{\max,g}\cdot f(r)=2u_{m,g}\cdot f(r) \tag{5.10}$$

$$f(r)=\left[1-\left(\frac{r_o}{r_e}\right)^2\right]\cdot\left[\frac{\left(\frac{r}{r_e}\right)^2-\left(\frac{r_o}{r_e}\right)^2+2\cdot\ln\left(\frac{r_o}{r}\right)}{3+\left(\frac{r_o}{r_e}\right)^4-4\cdot\left(\frac{r_o}{r_e}\right)^2+4\cdot\ln\left(\frac{r_o}{r_e}\right)}\right] \tag{5.11}$$

where r_e is the free surface radius defined as:

$$r_e = \left(\frac{1}{\varphi}\right)^{0.5} \cdot r_o \tag{5.12}$$

and φ is the fiber packing density, calculated as:

$$\varphi = \frac{n \cdot r_o^2}{r_{cont}^2} \tag{5.13}$$

where n is the number of fibers and r_{cont} is the radius of the hollow fiber contactor. The boundary conditions are the following.

$$r = r_e, \quad \frac{\partial C_{A,feed}}{\partial r} = 0; \quad \text{(symmetry condition)} \tag{5.14a}$$

$$r = r_o, \quad D_{A,feed}\frac{\partial C_{A,feed}}{\partial r} = k_m \cdot S \cdot \left(C_{A,feed} - C_A^*\right); \tag{5.14b}$$

$$z = 0, \quad C_{A,feed} = C_{A,in} \tag{5.14c}$$

where $D_{A,\,feed}$ is the diffusion coefficient of component A in the feed phase, S is a geometric factor based on the outer radius, and C_A^* is the concentration of component A in the feed phase in equilibrium with the receiving phase at the membrane-liquid interface.

According to Eq. (5.14b), the mass transfer through the membrane is described in terms of a mass transfer coefficient (k_m) which involves the assumption of a single resistance of the membrane and linear profile of concentration through the thickness of the membrane.

The differential mass balance in Eq. (5.9) can be converted to dimensionless by introducing the following dimensionless variables (Luis et al., 2010):

$$\theta = \frac{r}{r_o}, \quad \overline{z} = \frac{z}{L}, \quad \overline{C}_A = \frac{C_{A,feed}}{C_{A,in}} \tag{5.15a}$$

$$Sh_m = \frac{k_m \cdot S \cdot r_o}{D_{A,feed}} \quad \text{(Sherwood number)} \tag{5.15b}$$

$$Gz_{ext} = \frac{u_{m,g} d_o^2}{D_{A,feed} L} \quad \text{(Graetz number in the shell side, with } d_o = 2r_o\text{)} \tag{5.15c}$$

The resulting dimensionless mass balance and boundary conditions are:

$$\frac{Gz_{ext}}{2} \cdot f(\overline{r}) \cdot \frac{\partial \overline{C}_A}{\partial \overline{z}} = \frac{1}{\theta}\frac{\partial}{\partial \theta}\left(\theta \frac{\partial \overline{C}_A}{\partial \theta}\right) \tag{5.16}$$

$$f(\overline{r}) = \left[1 - \left(\frac{r_o}{r_e}\right)^2\right] \cdot \left[\frac{\left(\frac{\overline{r} \cdot r_o}{r_e}\right)^2 - \left(\frac{r_o}{r_e}\right)^2 + 2 \cdot \ln\left(\frac{1}{\overline{r}}\right)}{3 + \left(\frac{r_o}{r_e}\right)^4 - 4 \cdot \left(\frac{r_o}{r_e}\right)^2 + 4 \cdot \ln\left(\frac{r_o}{r_e}\right)}\right] \tag{5.17}$$

$$\theta = \frac{r_e}{r_o}, \quad \frac{\partial \overline{C}_A}{\partial \theta} = 0 \tag{5.18a}$$

$$\theta = 1, \quad \frac{\partial \overline{C}_A}{\partial \theta} = Sh_m \cdot \left(\overline{C}_A - \overline{C}_{A,rec}\right) \tag{5.18b}$$

$$\overline{z} = 0, \quad \overline{C}_A = 1 \tag{5.18c}$$

Inside the fiber

Inside the fiber or lumen side, the following assumptions can be considered: (1) Steady state and isothermal condition, (2) no axial diffusion, (3) fully developed parabolic velocity profile in the hollow fiber, (4) the physical properties of the fluid were constant, and (5) constant tube side pressure. Considering these assumptions, the mass conservation equation inside hollow fibers is given as (Bird et al., 2002):

$$u_{z,l}\frac{\partial C_{A,rec}}{\partial z} = D_{A,rec}\left[\frac{1}{r}\frac{\partial}{\partial r}\left(r\frac{\partial C_{A,rec}}{\partial r}\right)\right] \tag{5.19}$$

When the velocity is fully developed in a laminar flow, the axial velocity can be written as.

$$u_{z,l} = u_{\max,l}\left[1 - \left(\frac{r}{r_i}\right)^2\right] = 2u_{m,l}\left[1 - \left(\frac{r}{r_i}\right)^2\right] \tag{5.20}$$

Eq. (5.19) can be rewritten as:

$$2u_{m,l}\left[1 - \left(\frac{r}{r_i}\right)^2\right]\frac{\partial C_{A,rec}}{\partial z} = D_{SO_2,l}\left[\frac{1}{r}\frac{\partial}{\partial r}\left(r\frac{\partial C_{A,rec}}{\partial r}\right)\right] \tag{5.21}$$

The boundary conditions are the following.

$$r = 0, \quad \frac{\partial C_{A,rec}}{\partial r} = 0 \quad \text{(symmetry condition)} \tag{5.22a}$$

$$r = r_i, \quad D_{SO_2,l}\frac{\partial C_{A,rec}}{\partial r} = D_{SO_2,g}\frac{\partial C_{A,rec}}{\partial r} \tag{5.22b}$$

$$z = L, \quad C_{A,rec} = 0 \tag{5.22c}$$

where $D_{A,rec}$ is the diffusion coefficient of the component A in the receiving phase. It is assumed that the receiving phase does not have or have a negligible quantity of component A at the inlet of the contactor ($z = L$).

The bulk average or "mixing cup" values of component A concentration in the receiving phase at $z = 0$ (contactor outlet) is defined as.

$$C_{A,z=0}=\frac{\int_0^{r_i} C_{A,rec}u_{z,l}2\pi r\,dr}{\int_0^{r_i} u_{z,l}2\pi r\,dr}=\frac{4}{r_i^2}\int_0^{r_i} C_{A,rec}\left[1-\left(\frac{r}{r_i}\right)^2\right]r\,dr \tag{5.23}$$

The previous model equations can be rewritten in the dimensionless form as.

$$\frac{Gz_{\text{int}}}{2}\left[1-\overline{r}^2\right]\frac{\partial\overline{C}_{A,rec}}{\partial\overline{z}}=\frac{1}{\overline{r}}\frac{\partial}{\partial\overline{r}}\left(\overline{r}\frac{\partial\overline{C}_{A,rec}}{\partial\overline{r}}\right) \tag{5.24}$$

with the boundary conditions.

$$\overline{r}=0,\quad \frac{\partial\overline{C}_{A,rec}}{\partial\overline{r}}=0 \tag{5.25a}$$

$$\overline{r}=1,\quad \frac{\partial\overline{C}_{A,rec}}{\partial\overline{r}}=\frac{\partial\overline{C}_A}{\partial\overline{r}}\cdot\frac{D_{A,feed}}{D_{A,rec}}\cdot H \tag{5.25b}$$

$$\overline{z}=1,\quad \overline{C}_{A,rec}=0 \tag{5.25c}$$

where the dimensionless variables are defined as.

$$\overline{r}=\frac{r}{r_i},\qquad \overline{z}=\frac{z}{L},\qquad \overline{C}_A=\frac{C_A}{C_{A,sat}} \tag{5.26a}$$

$$Gz_{\text{int}}=\frac{u_{m,l}d_i^2}{D_{A,rec}L}\quad\text{(Graetz number in the tube side, with } d_i=2r_i) \tag{26b}$$

The dimensionless mixing cup may be also rewritten as.

$$\overline{C}_{A,rec,\overline{z}=0}=4\int_0^1 \overline{C}_{A,rec}\left[1-\overline{r}^2\right]\overline{r}\,d\overline{r} \tag{5.27}$$

Membrane

The following equation can be used to describe the mass transport through the membrane, which considers that diffusion is the only mechanism for mass transport (Faiz and Al-Marzouqi, 2009):

$$D_{i,membrane}\left[\frac{\partial^2 C_{i,membrane}}{\partial r^2}+\frac{1}{r}\frac{\partial C_{i,membrane}}{\partial r}+\frac{\partial^2 C_{i,membrane}}{\partial z^2}\right]=0 \tag{5.28}$$

The diffusion coefficient inside the membrane pores, $D_{i,membrane}$, is defined as an effective diffusion in order to account for the membrane's porosity, ε, and tortuosity, τ:

$$D_{i,membrane}=\frac{D_i\cdot\varepsilon}{\tau} \tag{5.29}$$

The boundary conditions are given as.

$$\text{At } r = R_1, C_{i,membrane} = \frac{C_{i,lumen}}{m_i} \tag{5.30a}$$

$$\text{At } r = R_2, C_{i,membrane} = C_{i,shell} \tag{5.30b}$$

where m_i is the solubility of the component i in the receiving phase.

The mathematical description included in this section is a general way to account for the mass transfer that take place from the feed phase to the receiving phase through a porous membrane. Nevertheless, the kind of fluid (gas or liquid) and the kind of species to be transported generate specificity in the system. The next sections include particular aspects to consider for each kind of application in a membrane contactor.

5.3 MEMBRANE-BASED ABSORPTION

Using a membrane contactor to separate a gas-liquid interface is considered as a clean technology since dragging of drops of solvent is avoided. Solvent losses are thus reduced, gas and liquid flow rates can be independently controlled and a determined interfacial area is obtained. Normally, a hollow fiber contactor is used with gas and liquid flowing on opposite sides of the membrane. The fluid-fluid interface is formed at the mouth of the membrane pores. In order to keep that interface immobilized and stable and to work under conditions of no membrane wetting, a very small pressure drop across the membrane is required. A small overpressure may be needed at the gas phase so that membrane wetting is minimized, or at the liquid phase in order to avoid bubbling of gas into the liquid. The breakthrough pressure given by Eq. (5.1) should be taken into account. The membrane material and kind of solvent will determine the best operating conditions. In order to fill the pores with gas, hydrophobic membranes should be used when the absorption solvent is hydrophilic (e.g., a hydrophobic polymeric contactor for CO_2 capture using aqueous solutions) (El-Naas et al., 2010) and hydrophilic membranes with hydrophobic solvents (e.g., a hydrophilic ceramic contactor for SO_2 capture using *N*,*N*-dimethylaniline) (Luis et al., 2008). The liquid gives selectivity to the separation and it should have good chemical compatibility with the exposed materials and avoid membrane wettability in order to ensure a long-term application. Toxicity and volatility are also key aspects to be considered when selecting the solvent since if the solvent is very volatile, it will tend to go to the gas phase even if the liquid-gas contact takes place within the pores of the membrane. Ideal solvents are thus those with high affinity for the target compound, low volatility, and low (or none) toxicity. The desorption or recovery step that follows the absorption is also a critical point in the design of the overall process. If thermal absorption is considered, the solvent should have low heat of absorption to decrease the energy during regeneration. If a solid product is envisaged, such as

carbonates or bicarbonates, posttreatment of the precipitated solid should be considered. An integrated approach using membrane contactors has been proposed in the literature in order to capture carbon dioxide and produce pure crystals of sodium carbonate. Membrane-based absorption and membrane distillation-crystallization have been integrated to achieve this purpose (Ye et al., 2013, 2016; Li et al., 2016; Ruiz-Salmón et al., 2017; Ruiz-Salmón and Luis, 2018). Indeed, one application of membrane contactors in gas-liquid systems that is currently leading the research on this technology is capture of carbon dioxide, mainly for postcombustion capture (i.e., CO_2/N_2 separation). CO_2 is transferred from the gas phase through the porous membrane to the liquid phase due to a driving force based on differences in concentration. Examples of absorption solvents used for CO_2 capture in membrane contactors are diethylamine (DEA), monoethylamine (MEA), aqueous solutions of alkaline salts, amino acids, or enzymes. Other applications are removal of other acid gases from gas streams (e.g., SO_2, H_2S) or volatile organic compounds.

The core of the experimental system to perform membrane-based absorption is the membrane contactor. Fig. 5.5 shows a typical experimental setup. The gas and liquid streams are introduced (normally) in countercurrent. Mass flow controllers can be used to control accurately the flow rate of the gas phase. The gas may flow inside the pores and the liquid outside or vice versa. The liquid phase can be recycled, taking into account that a pseudo steady state can be achieved. The gas phase is analyzed at the outlet of the contactor as well as the liquid phase, if required to check the mass balance. Some pretreatment of the gas phase may be required prior to be sent to the analyzer in order to eliminate interferences in the measurements, mainly if a volatile solvent is used.

The transmembrane flux can be calculated for the gas and the liquid phases according to these equations:

$$J_{A,g} = \frac{Q_g}{A}\left(C_{A,g}^{IN} - C_{A,g}^{OUT}\right) \tag{5.31a}$$

$$J_{A,l} = \frac{V_L}{A \cdot \Delta t}\left(C_{A,l,t+\Delta t} - C_{A,l,t}\right) \tag{5.31b}$$

where Q_g is the gas flow rate, A is the membrane area, and V_L is the total volume of absorption liquid in the system. Since the liquid is recycled into the process, $J_{A,l}$ is calculated considering the experimental concentration in a period of time Δt. At steady state, both gas and liquid fluxes should be equal. The mass transfer takes place by diffusion across the interface and the driving force for separation is a concentration gradient based on the solubility of the gas component into the liquid phase. As indicated in Section 5.2, the mass transfer through the membrane can be described by definition of an overall mass transfer coefficient, $K_{overall}$. This coefficient can be experimentally evaluated from the flux through the membrane calculated from Eqs. (5.31a) or (5.31b). Since $J_{A,g} = J_{A,l} = J_A$:

$$K_{overall} = \frac{J_A}{\Delta y_{lm}\left(P_T/RT\right)} \tag{5.32}$$

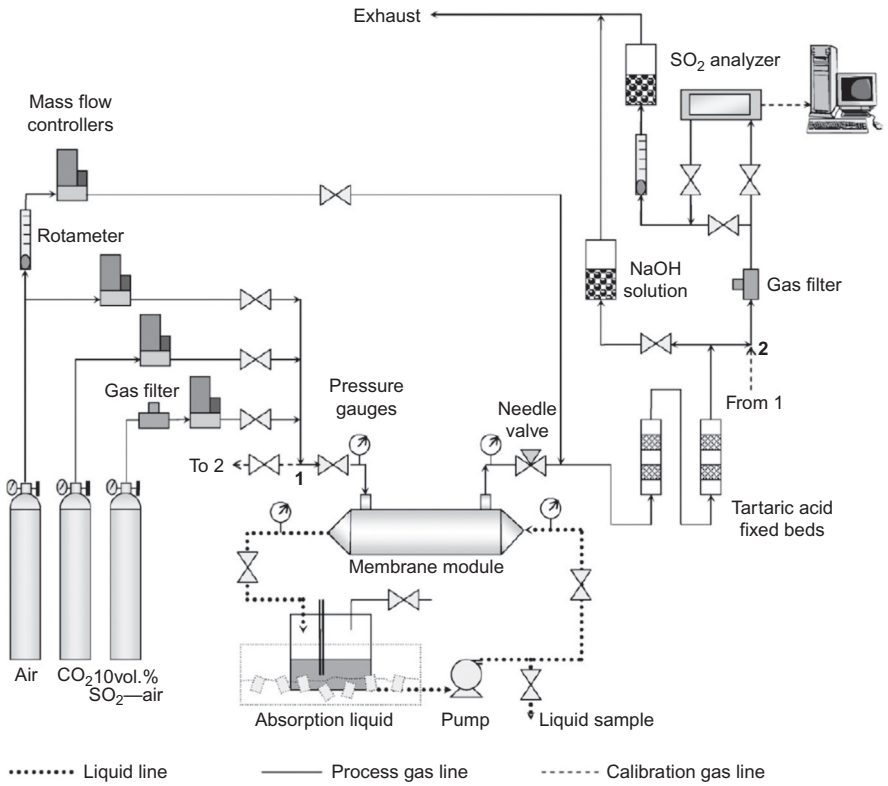

FIG. 5.5

Experimental setup for membrane-based gas absorption. Example of removal of SO_2 from a gas stream using dimethylaniline. Beds of tartaric acid are used to remove traces of solvent found in the gas stream before analysis.

Reproduced with permission from Luis, P., Garea, A., Irabien, A., 2009. Zero solvent emission process for sulfur dioxide recovery using a membrane contactor and ionic liquids. J. Membr. Sci. 330, 80–89.

P_T is the total pressure in the gas phase and Δy_{lm} is the logarithmic mean of the driving force based on gas phase molar fractions and taking into account the concentration of i at the inlet ($y_{i(g),in}$) and the outlet ($y_{i(g),out}$) of the contactor:

$$\Delta y_{lm} = \frac{\left(y_{i(g),in} - y^*_{in}\right) - \left(y_{i(g),out} - y^*_{out}\right)}{\ln\left(\dfrac{y_{i(g),in} - y^*_{in}}{y_{i(g),out} - y^*_{out}}\right)} \tag{5.33}$$

If the concentration of i in the liquid phase is very far from the saturation value, y^*_{in} and y^*_{out} in Eq. (5.33) can be considered negligible since the influence of the gas-liquid equilibrium is insignificant.

The removal efficiency of the target compound i (%) is defined by the following equation:

$$Removal\ \ efficiency = \left(1 - \frac{C_{A,g}^{OUT}}{C_{A,g}^{IN}}\right) \tag{5.34}$$

The removal efficiency together with the transmembrane flux gives information on the process performance. On the other hand, the overall mass transfer coefficient allows evaluating the membrane performance. Thus evaluating the overall mass transfer coefficient is of utmost interest to determine the degree of application of this technology and to compare with conventional absorption systems (absorption columns). In addition, the overall mass transfer coefficient will have a direct impact on the membrane area required for the separation. Fig. 5.6 shows an example for CO_2 capture. The higher the mass transfer coefficient, the lower the area. Overall mass transfer coefficients ranging between 10^{-5} and $10^{-3}\,m\,s^{-1}$ are common in this technology, involving contactors with a membrane area of around 10^5–$10^7\,m^2$ to capture $10^5\,t\ CO_2$ per year and reaching an outlet gas stream with <0.1 vol% CO_2 (Luis and Van der Bruggen, 2013).

According to Eq. (5.32), if a plot of the transmembrane flux versus the driving force is done, a straight line should be obtained, whose slope is the overall mass transfer coefficient, as shown in Fig. 5.7. If a linear relationship is not obtained, the overall mass transfer coefficient varies with the driving force, which may be due to phenomena of concentration polarization. Physically, it means that a higher

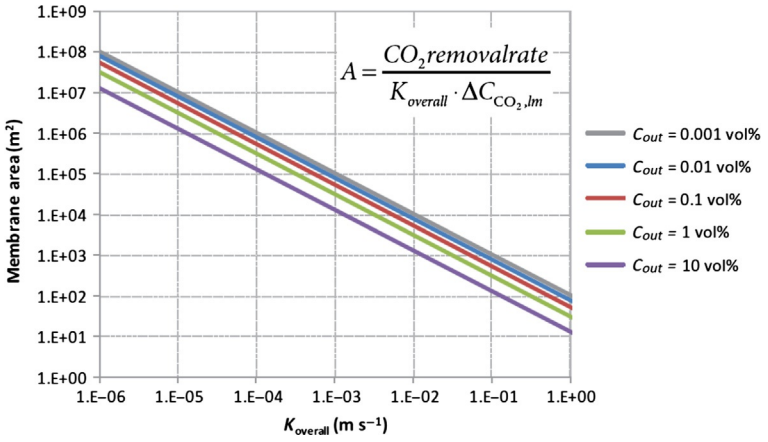

FIG. 5.6

Membrane area versus the overall mass transfer coefficient of a membrane contactor. C_{out} refers to the concentration (vol%) of CO_2 in the gas product. CO_2 removal rate = 1.105 tons of CO_2 per year ($1.61\,m^3\,s^{-1}$); feed concentration = 15 vol% CO_2.

Reproduced with permission from Luis, P., Van der Bruggen, B., 2013. The role of membranes in postcombustion CO_2 capture. Greenhouse Gas Sci. Technol. 3, 1–20. https://doi.org/10.1002/ghg.

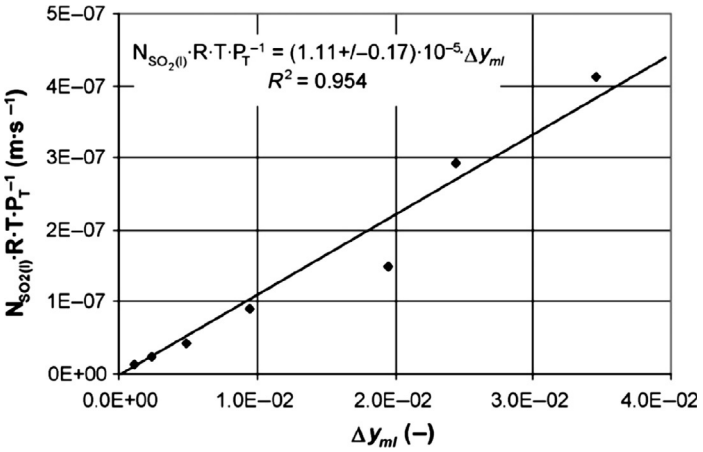

FIG. 5.7

Absorption flux ($N_{SO2(l)}$) versus sulfur dioxide logarithmic mean molar fraction (Δy_{ml}) in a membrane contactor to capture SO_2 using *N,N*-dimethylaniline is used as absorption liquid. *Reproduced with permission from Luis, P., Garea, A., Irabien, A., 2009. Zero solvent emission process for sulfur dioxide recovery using a membrane contactor and ionic liquids. J. Membr. Sci. 330, 80–89.*

driving force does not produce a higher transmembrane flux. Nevertheless, in gas-liquid systems, concentration polarization is less common.

The experimental overall mass transfer coefficient obtained from Eq. (5.32) or graphically as indicated in Fig. 5.7 can be compared with that obtained by applying the resistance-in-series model explained in Section 5.2. In a gas-liquid system, the membrane pores should be filled with gas in order to minimize the mass transfer resistance within the membrane pores. However, membrane wetting may take place, leading to a significant increase of the membrane resistance. The resistance-in-series model splits the overall mass transfer coefficient, $K_{overall}$, as a combination of the membrane mass transfer coefficient, k_{mg} for gas filled pores (nonwetted mode) or k_{ml} for liquid filled pores (wetted mode), and the liquid side, k_l, and gas side, k_g, mass transfer coefficients, according to Fig. 5.8A. Eq. (5.6) in Section 5.2 can be completed by adding the enhancement factor, E, since a chemical reaction in the liquid side takes place ($E=1$ for physical absorption), and the inner, outer, and mean-logarithmic diameters of the hollow fiber in order to take into account the system geometry (Yang et al., 2006; Luis et al., 2009):

$$\frac{1}{K_{overall}} = \frac{1}{k_g} + \frac{d_o}{k_{mg} \cdot d_{lm}} + \frac{H \cdot d_o}{k_l \cdot d_i \cdot E} \quad \text{Non} - \text{wetted mode} \tag{5.35a}$$

or

$$R_{overall,g} = R_g + R_{mg} + R_l \tag{5.35b}$$

The individual mass transfer coefficient for the membrane, k_m, can be calculated as the ratio of an effective diffusivity and the membrane thickness using Eq. (5.36):

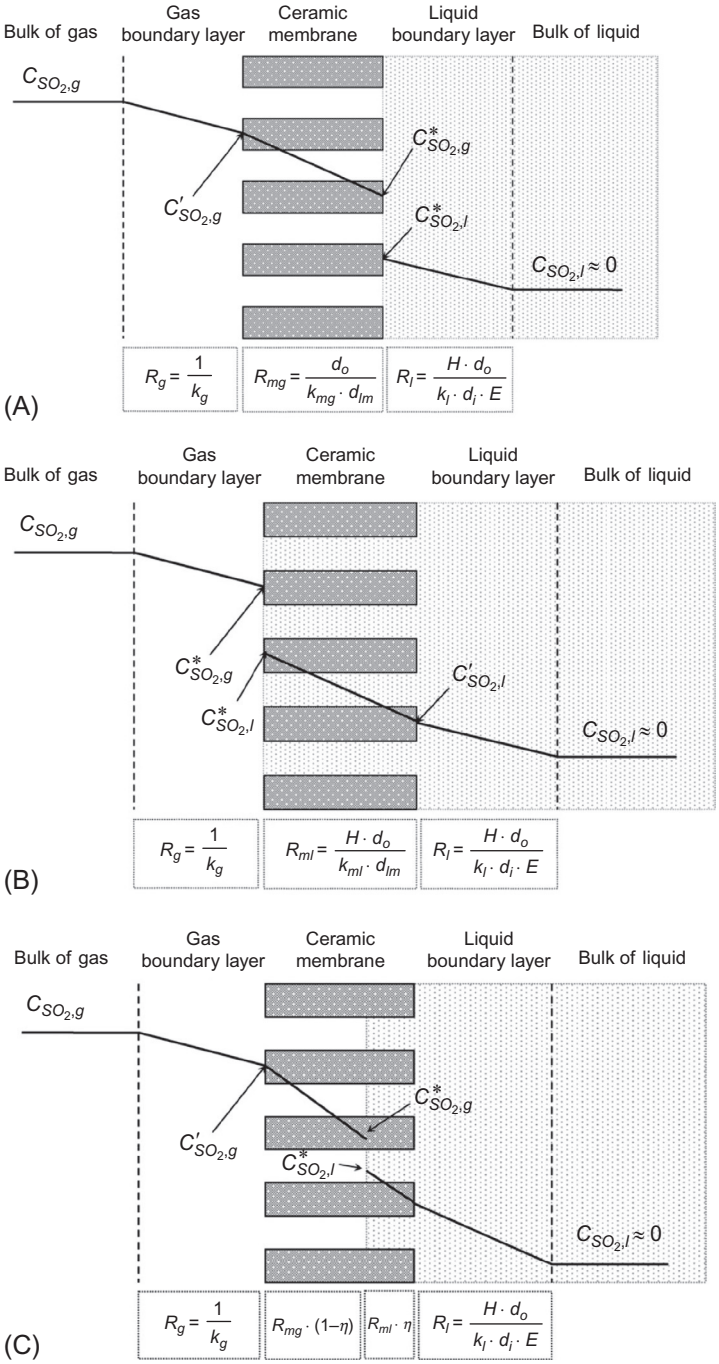

FIG. 5.8

Schematic diagram of mass transfer. Mass transfer through the porous membrane and local concentrations in membrane-based gas absorption of SO_2: (A) nonwetted mode; (B) wetted mode; (C) partially wetted mode.

Reproduced with permission from Luis, P., Garea, A., Irabien, A., 2009. Zero solvent emission process for sulfur dioxide recovery using a membrane contactor and ionic liquids. J. Membr. Sci. 330, 80–89.

$$k_{mg} = \frac{D_{eff,g}}{\delta} = \frac{D_{A,g} \cdot \varepsilon}{\tau \cdot \delta} \tag{5.36}$$

Nonwetting is a theoretical situation, thus it is possible to consider that the overall mass transfer coefficient obtained with Eq. (5.35a) is the maximum value. If wetting occurs, the experimental value will be smaller.

For gas flowing outside parallel to the hollow fiber, the mass transfer coefficient in the gas phase can be estimated from (Cussler, 1997)

$$\frac{k_g \cdot d_h}{D_{A,g}} = 1.25 \cdot \left(\frac{d_h^2 \cdot v_g}{L \cdot v}\right)^{0.93} \cdot \left(\frac{v}{D_{A,g}}\right)^{1/3} \tag{5.37}$$

$$d_h = \frac{d_{cont}^2 - n \cdot d_o^2}{n \cdot d_o} \tag{5.38}$$

where d_h is the hydraulic diameter, $D_{A,g}$ is diffusion coefficient in the gas phase, L is the fiber length, and υ is the kinematic viscosity. When the flow inside the hollow fiber is laminar, the mass transfer coefficient in the tube (liquid phase) is given by the Lévêque equation (Cussler, 1997):

$$\frac{k_l \cdot d_i}{D_{A,l}} = 1.62 \cdot \left(\frac{d_i^2 \cdot v_l}{L \cdot D_{A,l}}\right)^{1/3} \tag{5.39}$$

where d_i is the internal fiber diameter, and $D_{A,l}$ is the diffusion coefficient in the liquid phase.

The description of mass transfer by means of differential equations instead of resistance-in-series can be done as indicated in Section 5.2. Some considerations on membrane wetting are included later for both methods.

5.3.1 COMMENTS ON MEMBRANE WETTING IN THE RESISTANCE-IN-SERIES MODEL

The use of membrane contactors has shown typically membrane wetting after some time of operation. Mathematically, one could calculate an individual mass transfer coefficient for the membrane considering that the membrane pores are filled with liquid (Fig. 5.8B). This calculation would lead to the minimum overall mass transfer coefficient. Thus for the wetted mode, the overall mass transfer coefficient is calculated from:

$$\frac{1}{K_{overall}} = \frac{1}{k_g} + \frac{H \cdot d_o}{k_{ml} \cdot d_{lm}} + \frac{H \cdot d_o}{k_l \cdot d_i \cdot E} \quad \text{Wetted mode} \tag{5.40a}$$

or

$$R_{overall,l} = R_g + R_{ml} + R_l \tag{5.40b}$$

where d_o, d_i, and d_{lm} are the outside, inside, and log mean diameters of the hollow fiber. For a porous membrane wetted by the membrane, the mass transfer through the membrane is calculated as the effective diffusion coefficient, D_{eff}, of the absorbing

gas divided by the membrane thickness (Cussler, 1997; Gabelman and Hwang, 1999):

$$k_m = k_{ml} = \frac{D_{eff,l}}{\delta} = \frac{D_{SO_2,l} \cdot \varepsilon}{\tau \cdot \delta} \tag{5.41}$$

However, the real situation may be a partially wetted membrane. In this case, the overall mass transfer coefficient will be a value between the $K_{overall}$ obtained under nonwetted conditions and totally wetted conditions. The mechanism of partial wetting can be used to explain the results according to the method proposed in recent studies (Lu et al., 2005; Lu et al., 2008). It is based on considering that the membrane resistance is a function of the resistance of pores filled with gas and pores filled with liquid. The membrane resistance can be separated in two new resistances according to Eq. (5.38) and Fig. 5.8C:

$$\frac{1}{K_{overall}} = \frac{1}{k_g} + \frac{1}{k_{mg}} \cdot \frac{d_o}{d_{lm}} \cdot (1-\eta) + \frac{H}{k_{ml}} \cdot \frac{d_o}{d_{lm}} \cdot \eta + \frac{H \cdot d_o}{k_l \cdot d_i \cdot E} \quad \text{Partial wetting} \tag{5.42a}$$

or

$$R_{overall} = R_g + R_{mg} \cdot (1-\eta) + R_{ml} \cdot \eta + R_l \tag{5.42b}$$

where η is the wetting ratio defined as a ratio of the pore length wetted by liquid to the total length.

An example of this methodology can be found in Luis et al. (2009) for absorption of SO_2 using a ceramic membrane contactor and *N*,*N*-dimethylaniline or the ionic liquid 1-ethyl-3-methylimidazolium ethylsulfate ([EMIM][$EtSO_4$]) as the absorption liquids. The authors found a significant difference between the estimated mass transfer coefficients when pores are filled with gas and the experimental overall mass transfer coefficients when using both solvents. The discussion was focused on partial wetting of the membrane. The wetting fraction η took a value of around 74% and 4% when *N*,*N*-dimethylaniline and [EMIM][$EtSO_4$] were used, respectively. This large difference of wetting depending of the used solvent was explained in terms of difference of viscosity. The ionic liquid has a viscosity of 97.6×10^{-3} Pa s (Gómez et al., 2006; Ranke et al., 2007) compared to the viscosity of *N*,*N*-dimethylaniline (1.20×10^{-3} Pa s), which would make more difficult the wetting of the membrane. In addition, capillary condensation of *N*,*N*-dimethylaniline into the pores could increase the wetting phenomenon.

5.3.2 COMMENTS ON MEMBRANE WETTING IN THE MODEL BASED ON DIFFERENTIAL EQUATIONS

If the absorption liquid penetrates into the membrane pores, a mathematical model that considers gas inside the pores will lead to a poor interpretation of the reality. Partial wetting can be considered by dividing the membrane in two sections: a gas-filled section and a liquid-filled section.

Gas-filled section. The material balance for this section can be considered to be due to diffusion in the gas phase (Fig. 5.9):

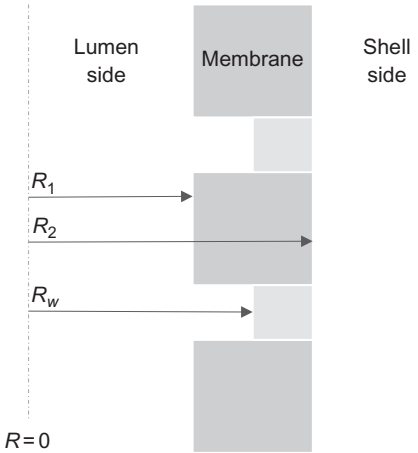

FIG. 5.9

Schematic diagram of membrane wetting and radial coordinates.

$$D_{i,g-membrane}\left[\frac{\partial^2 C_{i,g-membrane}}{\partial r^2}+\frac{1}{\mathrm{r}}\frac{\partial C_{i,g-membrane}}{\partial r}+\frac{\partial^2 C_{i,g-membrane}}{\partial z^2}\right]=0 \tag{5.43}$$

With the boundary conditions:

$$\text{At } r=R_w, C_{i,g-membrane}=\frac{C_{i,l-membrane}}{m_i} \tag{5.44a}$$

$$\text{At } r=R_2, C_{i,g-membrane}=C_{i,shell} \tag{5.44b}$$

Liquid-filled section. The portion of the membrane wetted by the liquid can be described by considering diffusion and reaction in the liquid phase:

$$D_{i,l-membrane}\left[\frac{\partial^2 C_{i,l-membrane}}{\partial r^2}+\frac{1}{r}\frac{\partial C_{i,l-membrane}}{\partial r}+\frac{\partial^2 C_{i,l-membrane}}{\partial z^2}\right]+R_{i,membrane}=0 \tag{5.45}$$

The reaction takes place inside the membrane pores. Therefore the porosity should be considered in the reaction term:

$$R_{i,membrane}=R_i\cdot\varepsilon \tag{5.46}$$

The boundary conditions are:

$$\text{At } r=R_1, C_{i,l-membrane}=C_{i,lumen} \tag{5.47a}$$

$$\text{At } r=R_w, C_{i,l-membrane}=C_{i,g-membrane}\cdot m_i \text{ for the absorbed species} \tag{5.47b}$$

$$\frac{\partial C_{i,membrane}}{\partial r}=0 \text{ for the nonabsorbed species} \tag{5.47c}$$

Alternatively, a mass transfer coefficient k_m whose inverse represents the resistance to mass transfer caused by the membrane can be defined, as indicated in the resistance-in-series model. If membrane pores are assumed to be filled with gas, a theoretical value k_{mg} could be calculated according to Eq. (5.36). The dimensionless equation containing the mass transfer coefficient in the membrane is then represented by the Sherwood number Sh_{mg}:

$$Sh = \frac{k_{mg} Sr_o}{D_{A,g}} \tag{5.48}$$

where k_{mg} is the theoretical mass transfer coefficient of the nonwetted membrane. When membrane wetting takes place, the Henry's law coefficient, H, and the fraction of wetting would have to be considered in the calculations. However, there is a lack of certainty in those parameters. A strategy could be to define an "effective" Sherwood number that includes the uncertainty: $Sh_{eff} = Sh/H$.

5.4 MEMBRANE-BASED SOLVENT EXTRACTION

Membrane-based solvent extraction or nondispersive solvent extraction is an alternative of classical solvent extraction where mass transfer between immiscible liquids occurs at the immobilized L-L interface at the mouth of pores of a microporous wall (Schlosser et al., 2005). This technology has been considered as a useful modern technique for metals extraction, recovery and separation of organic acids and isomers, and more generally, in chemical and pharmaceutical technology, biotechnology, food processing, and environmental engineering (Younas et al., 2011; Raynie, 2006; Schlosser et al., 2005; San Román et al., 2010). The solvent has to be regenerated in order to reuse it and recover the solute. The extraction can be done using also membrane contactors and a stripping solution or by other methods such as distillation. Fig. 5.10A shows the principle of membrane-based extraction. The membrane, filled with the solvent, separates effectively the feed solution and the solvent, occurring the transfer of solute through the membrane from the feed to the solvent phase.

Another process that is based on the same principles that membrane-based extraction is pertraction through a liquid membrane where both extraction and stripping of the solute take place in the same equipment (Schlosser et al., 2001, 2005). The liquid membrane can be in the configuration of a supported liquid membrane (the solvent is kept within the membrane pores) (Fig. 5.10B), or as a bulk liquid membrane (Fig. 5.10C), in which the membrane stability is not a problem like when using supported liquid membranes but a higher mass transfer resistance is expected due to a thicker liquid membrane layer between walls (Schlosser et al., 2001).

The mass transfer through the membrane is produced due to several mechanisms: physical solubility of the solutes into the solvent, or chemical or biochemical reactions. To find the appropriate extractant is a difficult task. Several aspects should be fulfilled. First, the complex formed by the solute and extractant has to be soluble in

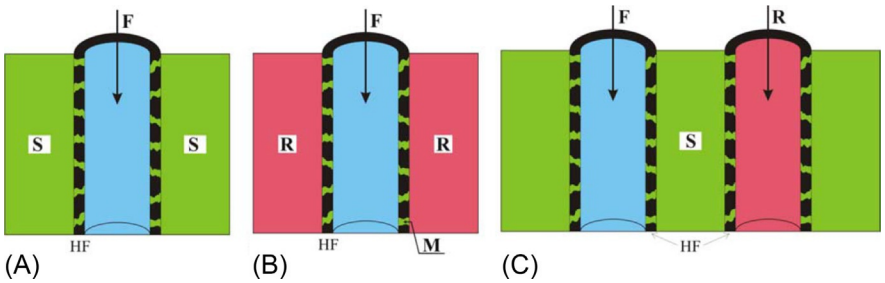

FIG. 5.10

Processes with immobilized L-L interface(s). (A) Membrane-based solvent extraction; (B) pertraction through supported liquid membrane; (C) pertraction through bulk liquid membrane with two immobilized L-L interfaces in a hollow fiber contactor. *F*, feed (donor) phase; *HF*, hollow fiber (microporous, hydrophobic); *M*, membrane phase; *R*, stripping (acceptor) solution; *S*, solvent.

Reproduced with permission from Schlosser, S., Kertész, R., Marták, J., 2005. Recovery and separation of organic acids by membrane-based solvent extraction and pertraction. An overview with a case study on recovery of MPCA. Sep. Purif. Technol. 41, 237–266.

the diluent that forms with the extractant a solvent. The selection of an adequate diluent or addition of a modifier to the solvent could be necessary. The diluent type may have a great influence on the solvent performance. Furthermore, the composition of the feed and its pH can have a significant influence in the transport rate in extraction. If there are components that compete with the target solute(s), the transport rate will decrease. Thus the presence of those compounds should be avoided or kept at minimum concentration. The transport rate will be also decreased by the adsorption of surfactants on the liquid-membrane interface. The kind of the stripping reagent and its concentration in the stripping solution may also affect the process performance. The most important is to have an excess of reagent and to avoid the formation of a boundary layer depleted in the reagent (Schlosser et al., 2005).

A typical experimental setup used in membrane-based liquid extraction is shown in Fig. 5.11. It consists basically of two reservoirs for the feed and extractant solutions and the membrane contactor. Control of the flow rates and pressures is required to evaluate correctly the process performance. Commonly, periodic samples are taken from the feed tank in order to evaluate the variation of concentration over time, which allows calculating the amount of component that is extracted.

The mass transfer analysis in the hollow fiber contactor is based on the Fick's law of diffusion and film theory as explained in Section 5.2. The overall mass transfer coefficient, K_{aq}, is thus the main parameter to be determined:

$$J = K_{aq} A \left(C_{aq} - C_{aq}^{*} \right) \tag{5.49}$$

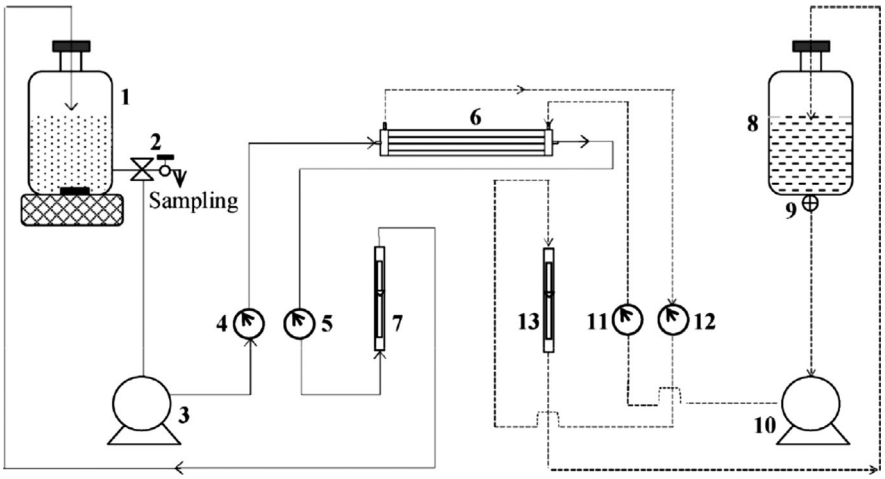

FIG. 5.11

Scheme of a typical experimental setup for membrane-based extraction using a hollow fiber membrane module. (1) SA-water tank with stirrer. (2) Valve and sampling port. (3) Gear pump (lumen side). (4) Pressure gauge (lumen side inlet). (5) Pressure gauge (lumen side outlet). (6) HFMC module. (7) Flowmeter (lumen side). (8) Extractant tank. (9) Flow control valve (extractant tank). (10) Gear pump (shell side). (11) Pressure gauge (shell side inlet). (12) Pressure gauge (shell side outlet). (13) Flowmeter (shell side).

Reproduced with permission from Agrahari, G.K., Pandey, N., Verma, N., Bhattacharya, P.K., 2014. Membrane contactor for reactive extraction of succinic acid from aqueous solution by tertiary amine. Chem. Eng. Res. Des. 92, 2705–2714.

where J is the mass flow rate of solute from aqueous phase to organic phase, A is the surface area of the membrane, C_{aq} is the concentration of solute in the aqueous phase at time "t," and C^*_{aq} is the hypothetical concentration of the solute in aqueous phase in equilibrium with organic phase at the same time. In this case, K_{aq} is based on the aqueous phase side but it could be defined similarly for the organic phase.

Evaluation of mass transfer coefficients is of most importance since they determine the rate at which equilibrium is approached, control the time required for a given separation and therefore the size and cost of the equipment to be used (Viegas et al., 1998). The overall mass transfer coefficient can be related to individual mass transfer coefficients at the aqueous phase side (k_{aq}), within the membrane (k_m), and at the organic phase side (k_{org}), following the resistance-in-series model described in Section 5.2. For aqueous phase flowing in flow-cell (outside the fiber) without chemical reaction or with instantaneous chemical reaction at the interface (Younas et al., 2011):

$$\frac{1}{K_{aq}} = \frac{1}{k_{aq}} + \frac{d_{ext}}{Pk_m d_{lm}} + \frac{d_{ext}}{Pk_{org} d_{int}} \tag{5.50}$$

and for aqueous phase flowing inside the fiber of a hydrophobic membrane, based on aqueous phase side concentration and without chemical reaction or with instantaneous chemical reaction at the interface,

$$\frac{1}{K_{aq}} = \frac{1}{k_{aq}} + \frac{d_{int}}{Pk_m d_{lm}} + \frac{d_{int}}{Pk_{org} d_{ext}} \tag{5.51}$$

P is the partition coefficient defined as the ratio of solute concentration in organic phase to that in aqueous phase at equilibrium; d_{int} and d_{ext} are the inner and outer diameter of the fiber, respectively; d_{lm} is the logarithmic mean diameter. The calculation of the local mass transfer coefficients (k_{aq}, k_m, and k_{org}) can be done by using correlations similar to those shown in Eqs. (5.36), (5.37), and (5.39).

The first term of the right side in Eqs. (5.50) and (5.51) is the resistance produced by the aqueous phase; the second term is the resistance produced by the membrane; and the third term, the resistance produced by the extractant. In this way, the analysis of the importance of each resistance when varying the operating conditions can be performed. For example, Younas et al. (2011) determined the effect of flow rates and value of the partition coefficient on the mass transfer resistances for the extraction of copper (II) from aqueous solutions. Fig. 5.12A and B shows the results for a flow rate of 1.67×10^{-6} and 16.67×10^{-6} $m^3\ s^{-1}$ (for both the organic and the aqueous phase), respectively. As general conclusions, they observed that the partition coefficient, which changes with the type of diluents, is the foremost parameter for mass transfer resistance analysis. As the partition coefficient decreases, the mass transfer resistance offered by the membrane increases, although the viscosity of the extractive phase will have a significant effect as well, which could explain the variation to this general conclusion. Increasing the flow rate produces a significant decrease of the resistances produced by the fluid phases. Therefore the membrane contributes more to the total resistance. This is a clear indication of mass transfer limitations in the fluid phases which can be improved by increasing the turbulence, that is, increasing the flow rate.

The overall resistance of mass transfer (the inverse of the overall mass transfer coefficient) can be plotted as a function of the inverse of the fluid velocity, which is the typically used Wilson plot method. This method allows the determination of the addition of other resistances as well as its dependence with the fluid velocity. This method has some limitations since it only accepts one variable (the fluid velocity). However, its usefulness and interest has been demonstrated in the literature (Viegas et al., 1998; Coelhoso et al., 2000). Fig. 5.13 shows the Wilson plot method elaborated by Viegas et al. (1998) when the tube side Reynolds number is varied (Fig. 5.13A) and when the shell side Reynolds number is varied (Fig. 5.13B) in the removal of valeric acid from an aqueous phase. The intercepts are the complementary resistances of each side (the other side resistance plus the resistance of the membrane itself). This is a very simple way to evaluate the variation of mass transfer coefficients with the fluid velocity. However, this methodology involves large errors. Viegas et al. (1998) developed a new methodology that considers the

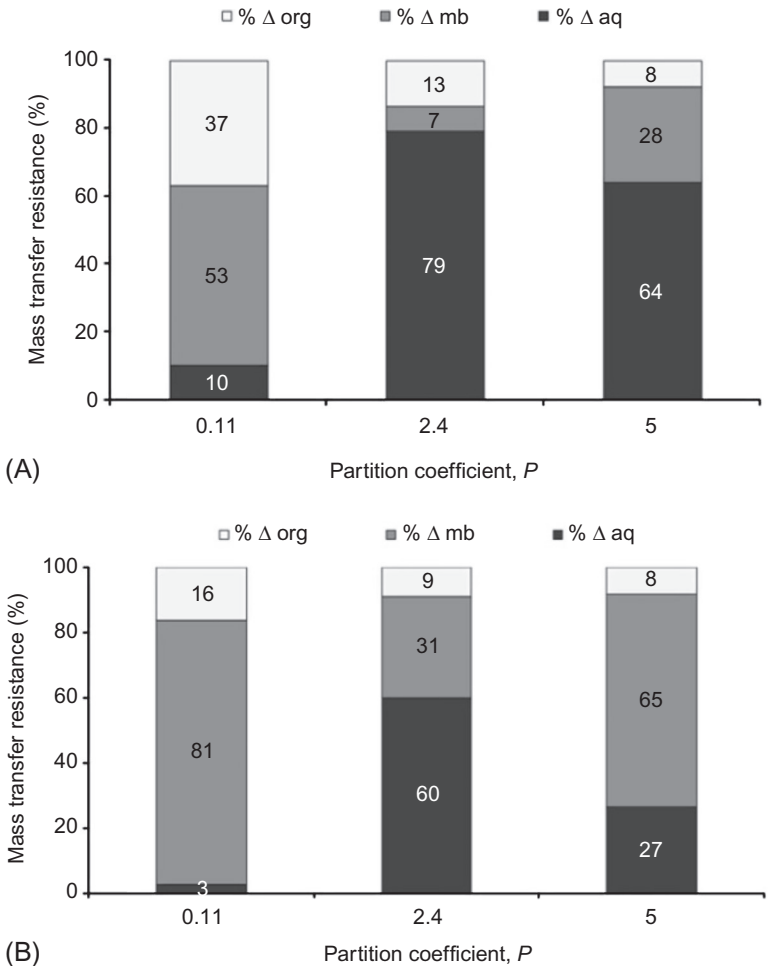

FIG. 5.12

Mass transfer resistance analysis for copper (II) extraction with TFA:
(A) $Q_{aq} = Q_{org} = 1.67 \times 10^{-6}\ m^3\ s^{-1}$; (B) $Q_{aq} = Q_{org} = 16.67 \times 10^{-6}\ m^3\ s^{-1}$.

partition coefficient as a function of time and concentration, achieving a single analytical expression. The Wilson plot methodology can be thus used acceptably to develop mass transfer correlations in systems operating in steady-state conditions and when the only variable is the fluid velocity. In systems where a parameter is a function of another variable or when operating in a transient state, the methodology proposed by Viegas et al. (1998) should be considered for a more accurate evaluation.

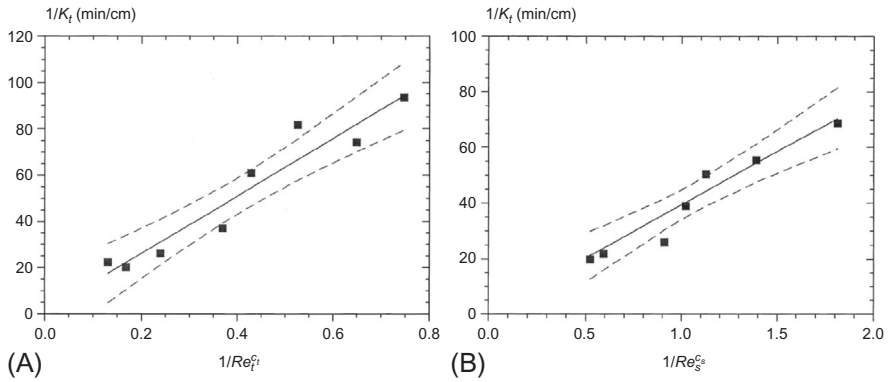

FIG. 5.13

Wilson plot representation considering a constant partition coefficient: (A) tube side and (B) shell side. Squares: experimental data; continuous line: model fitting; discontinuous line: 95% confidence limits.

Reproduced with permission from Viegas, R.M.C., Rodríguez, M., Luque, S., Alvarez, J.R., Coelhoso, I.M., Crespo, J.P.S.G., 1998. Mass transfer correlations in membrane extraction: analysis of Wilson-plot methodology. J. Membr. Sci. 145, 129–142.

5.5 MEMBRANE DISTILLATION-CRYSTALLIZATION

Membrane distillation is a novel alternative to separate mixtures containing volatile components. Like in distillation, vaporization of the feed solution is produced. However, the presence of the membrane generates a driving force based on a difference of concentration in addition to temperature. This driving force allows working at lower temperatures than conventional distillation without requiring reaching the boiling point of the feed mixture.

In membrane distillation, a microporous hydrophobic membrane is used since normally, the target separation is an aqueous solution and membrane wetting should be prevented. The feed aqueous solution is normally heated, although it is possible to work at room temperature if a concentration gradient is provided, for example, by using an osmotic solution (high concentrated solution of salts) at the permeate side. Typical feed temperatures vary in the range of 30–60°C. The volatile compounds in the feed solution evaporate and a vapor-liquid interface is created at the mouth of the pore. Those components diffuse and/or convect across the membrane pores, being condensed and/or removed on the opposite side of the membrane (permeate or distillate) (Curcio and Drioli, 2005). The hydrophobic character of the membrane prevents the inclusion of liquid inside the pores of the membrane in order to minimize its resistance to mass transfer. In addition, nonvolatile solutes are rejected and kept in the feed side.

Several configurations have been developed in membrane distillation depending on how the driving force is generated:

- Direct contact membrane distillation (DCMD): the permeate side of the membrane is a condensing fluid (commonly pure water) that is directly in contact with the membrane. The driving force is generated by the difference of temperature between the feed solution and the condensing fluid.
- Osmotic membrane distillation (OMD): an osmotic (high concentrated) solution is used at the permeate side to create a concentration-based driving force (vapor pressure difference between both membrane sides related to the water activities in the feed and osmotic solutions) to transfer water from the feed solution to the osmotic solution. The salts selected as osmotic pressure agents are normally NaCl (because of its low cost), $MgCl_2$, $CaCl_2$, and $MgSO_4$ (65). The temperature in the feed solution can be increased while keeping the osmotic solution at room (or lower) temperature to take advantage of the temperature gradient that is generated. As reference, when the osmotic evaporation is carried out at room temperature, transmembrane fluxes generally range between 0.2 and 0.4 $L/m^2 h$ are obtained (66). (Curcio and Drioli, 2005).
- Air gap membrane distillation (AGMD): the vaporized solvent is recovered on a condensing surface separated from the membrane by an air gap. The driving force is a concentration and/or temperature gradient across the membrane.
- Vacuum membrane distillation (VMD): vacuum is applied at the permeate side of the membrane. A large difference in partial pressure is produced thanks to the applied vacuum.
- Sweep gas membrane distillation (SGMD): a sweep gas is used at the other side of the membrane to recover the vaporized compound, establishing a difference in partial pressure across the membrane.

Membrane crystallization appears as an extension of the working principle of membrane distillation. As in membrane distillation, volatile solvents in the feed solution are evaporated and transfer through the membrane pores to the permeate side at the other side of the membrane. The objective is to concentrate the feed solution above their saturation limit, reaching a supersaturation that allows crystals to nucleate and grow. The role of the membrane in membrane crystallization is twofold. On one hand, it is the barrier that separates the feed phase from the permeate side, according to the characteristics of membrane contactors. On the other hand, the membrane acts as a solid support on which the solute molecules can converge forming clusters (nuclei) or growth units, leading to a heterogeneous nucleation. This is due to the decrease in the energetic barrier of nucleation, ΔG^*, that must be reached to induce the formation of stable nuclei. This energetic barrier is related to the minimum size of cluster (the critical nucleus, r^*) that have to be achieved to be likely to grow spontaneously. The nucleation barrier is calculated as (Curcio and Drioli, 2005):

$$\Delta G^* = \frac{16\pi v^2 \gamma^3}{3[kTlnS]^2} \tag{5.52}$$

where v is the molar volume occupied by a growth unit, γ the surface energy, and S the supersaturation. When the supersaturation S tends to 1, the energy barrier tends to infinite. Thus it is necessary to exceed the supersaturation value to observe spontaneous homogeneous precipitation. In addition, if a membrane is in contact with the crystallizing solution, the energy of nucleation decreases and heterogeneous nucleation may take place. The literature gives an equation to estimate the reduction of the energy produced when a substrate is present as a function of the contact angle θ formed between the solute and the substrate (membrane) (Curcio and Drioli, 2005):

$$\Delta G^{het} = \Delta G^{hom}\left[\frac{1}{2} - \frac{3}{4}cos\theta + \frac{1}{4}\cos^3\theta\right] \tag{5.53}$$

Three situations can be highlighted:

- $\theta = 180°$: the solution wets the substrate completely. In this case, both energies are coincident, $\Delta G^{het} = \Delta G^{hom}$;
- $\theta = 90°$: hydrophilic-hydrophobic limit. The energy of nucleation barrier for heterogeneous nucleation is half the value for homogeneous nucleation, $\Delta G^{het} = \frac{1}{2}\Delta G^{hom}$;
- $\theta < 90°$: hydrophobic membrane. The energy of nucleation barrier for heterogeneous nucleation is lower than the half of the value for homogeneous nucleation, $\Delta G^{het} < \frac{1}{2}\Delta G^{hom}$.

As consequence, the hydrophobic character of the membrane has an important relevance in the crystallization process. Fig. 5.14 shows the reduction in the energy barrier for several common membrane materials (Curcio and Drioli, 2005).

The transmembrane flux (J, $m^3\ m^{-2}\ s^{-1}$) of water through the membrane can be experimentally calculated by weighing the feed reservoir over time since a decrease of water is produced, concentrating the feed solution:

$$J(t_i) = -\frac{1}{A}\frac{dV_p}{dt} \approx -\frac{1}{A\rho_{water}}\frac{dw_f}{dt} = -\frac{1}{A\rho_{water}}\frac{w_f(t_{i+1}) - w_f(t_i)}{t_{i+1} - t_i} \tag{5.54}$$

where V_p (m^3) is the volume of water permeated from the feed solution to the permeate side, A (m^2) is the membrane area, ρ_{water} ($kg\,m^{-3}$) is the density of water, w_f (kg) is the weight of the reservoir containing the feed solution at time t_i (s).

If a concentration profile exists, as happens in osmotic membrane crystallization, the mass transfer from the feed to the osmotic solution is determined as the difference of water activity at both sides of the membrane. The overall mass transfer coefficient, K_{ov} ($m\,Pa^{-1}\ s^{-1}$), relates thus the transmembrane flux and the driving force (Ye et al., 2013; Li et al., 2014):

$$J = K_{ov}\left(p_f^* a_f - p_p^* a_p\right) \tag{5.55}$$

where J is the water flux calculated in Eq. (5.1); a is the water activity of the feed (f) and osmotic (p) side; and p_f^* and p_p^* are the water vapor pressures (Pa) of the feed and the osmotic solution, respectively. The water activity of a pure solution can be

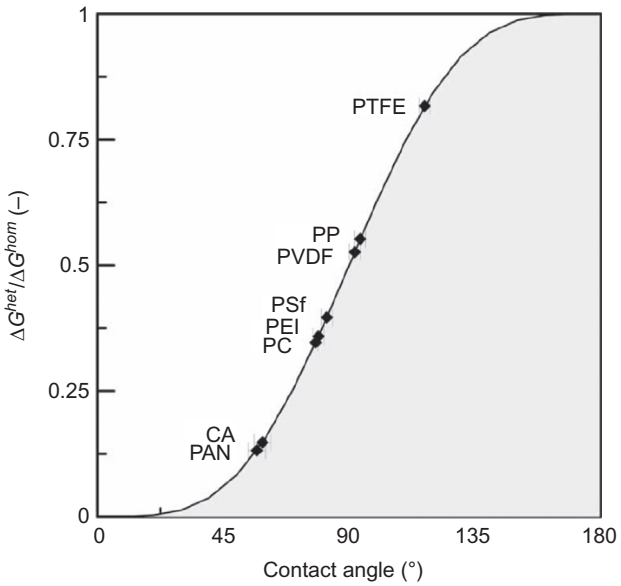

FIG. 5.14

Reduction in the free energy of the nucleation barrier due to heterogeneous nucleation as a function of the water contact angle with the polymeric surface (*CA*, cellulose acetate; *PAN*, polyacrylonitrile; *PC*, polycarbonate; *PET*, polyetherimide; *PES*, polyethersulfone; *PP*, polypropylene; *PSf*, polysulfone; *PTFE*, polytetrafluoroethylene; *PVDF*, polyvinylidenefluoride).

Reproduced with permission from Curcio, E., Enrico, D., 2005. Membrane distillation and related operations—a review. Sep. Purif. Rev. 34, 35–86.

calculated by Eqs. (5.3a), (5.3b) if the values of the osmotic coefficients are available in the literature, or by using the procedure described by Sandler (2006):

$$\varphi = \frac{-1000}{vmM} \ln a_w \tag{5.56}$$

where φ is the osmotic coefficient, v is the number of ions that the solute molecule dissociates in the solution, m is the molality ($\mathrm{mol\,kg^{-1}}$), M is the molar mass of the solvent, and a_w is the water activity. The vapor pressure of water (p^*) depends on the temperature (T) of the solution and it can be calculated by the Antoine equation (pressure in mm Hg and temperature in °C) (Luis et al., 2013):

$$p^*(T) = 10^{8.07131 - \frac{1730.63}{233.426 + T}} \tag{5.57}$$

Regarding the temperature gradient, an experimental heat transfer coefficient (U_{exp}, $\mathrm{W\,m^{-2}\,K^{-1}}$) can be calculated following a semiempirical procedure in which the heat by convection (Q_{conv}, $\mathrm{W\,m^{-2}}$) and conduction (Q_{cond}, $\mathrm{W\,m^{-2}}$) are involved (based on the equation described by Gryta et al. (1997)):

$$U_{exp} = \frac{Q_{conv} + Q_{cond}}{\Delta Tln} = \frac{J_w c_P \Delta T_b + \frac{k_{mem}}{\delta}\Delta T_w}{\Delta Tln} \tag{5.58}$$

where J_w is the permeate flux ($\mathrm{Kg\,m^{-2}\,s^{-1}}$), c_P is the heat capacity ($\mathrm{J\,kg^{-1}\,K^{-1}}$), k_m is the thermal conductivity of the membrane ($\mathrm{W\,m^{-1}\,K^{-1}}$), and δ is the membrane thickness (m); ΔTln, ΔT_b, ΔT_w are the logarithm mean temperature, the difference of temperature among the feed and the osmotic side in the bulk and in the membrane surface, respectively.

The resistance-in-series model is typically applied in membrane distillation-crystallization. Fig. 5.15 shows a scheme of the concentration and temperature profiles and the resistances in osmotic membrane distillation (Ruiz-Salmón and Luis, 2018).

The mass transfer coefficient inside the fibers (feed side) can be calculated from (Gabelman and Hwang, 1999):

$$k_f = \frac{Sh\, D_{Na_2CO_3,water}}{d_i} \tag{5.59}$$

$$Sh = 0.664 Re^{0.5} Sc^{0.33} \left(\frac{d_i}{l}\right)^{0.33} \tag{5.60}$$

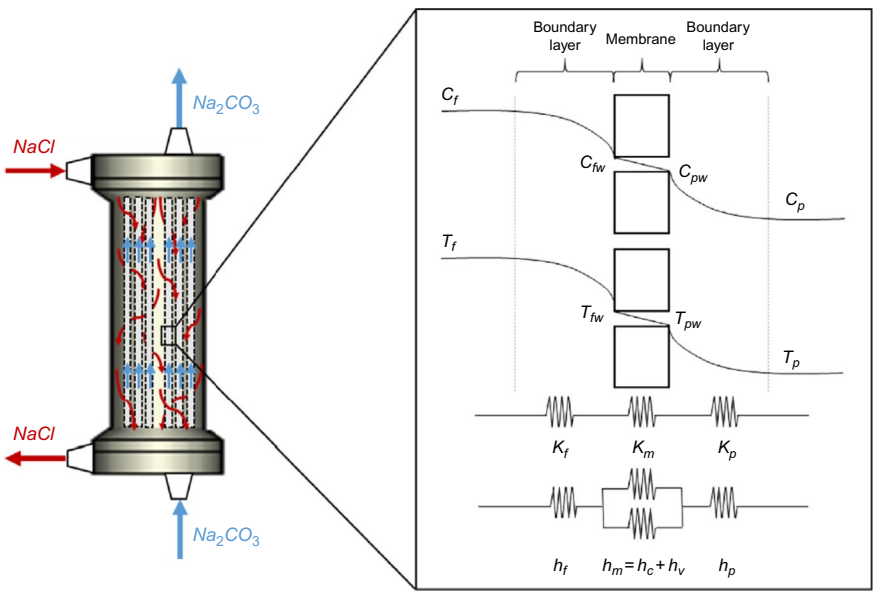

FIG. 5.15

Counter-current mode in osmotic membrane distillation (left) and mass and heat transfer resistances (right).

Reproduced with permission from Ruiz-Salmón, I., Luis, P., 2018. Membrane crystallization via membrane distillation. Chem. Eng. Process. Process Intensif. 123, 258–271.

$$\mathrm{Re} = \frac{\rho_f v_f d_i}{\eta_f} \tag{5.61}$$

$$Sc = \frac{\eta_f}{\rho_f D_{Na_2CO3,water}} \tag{5.62}$$

where Sh, Re, and Sc are the Sherwood, Reynolds, and Schmidt numbers, respectively; d_i (m) is the inside diameter of the fibers; ρ (kg m^{-3}) and η (Pa s), the density and the viscosity of the solution, respectively; v (m s^{-1}), the velocity of the fluid through the fibers and $D_{Na_2CO3,water}$ (m^2 s^{-1}) is the diffusivity of Na_2CO_3 in water.

The mass transfer coefficient at the shell side (osmotic solution) is calculated from (Gabelman and Hwang, 1999):

$$k_p = \frac{Sh\, D_{NaCl,water}}{d_h} \tag{5.63}$$

$$Sh = 5.8\left(\frac{d_{h(1-\phi)}}{l}\right) Re^{0.6} Sc^{0.33} \tag{5.64}$$

$$\mathrm{Re} = \frac{\rho_p v_p d_h}{p} \tag{5.65}$$

$$Sc = \frac{\eta_p}{\rho_p D_{NaCl,water}} \tag{5.66}$$

where l (m) is the length; d_h (m), the hydraulic diameter; and ϕ is the packing fraction of the fibers in the shell.

The mass transfer coefficient in the membrane is calculated from (Gabelman and Hwang, 1999):

$$k_m = \frac{1}{RT}\left(\frac{D_w^k D^\circ_{w-a}}{D^\circ_{w-a} + p_a D_w^k}\right)\left(\frac{M}{\delta}\right) \tag{5.67}$$

$$D_w^k = \frac{2\varepsilon r_p}{3\tau}\sqrt{\frac{8RT_{avg}}{\pi M}} \tag{5.68}$$

$$D^\circ_w(T) = -2.775\,10^{-6} + 4.479\,10^{-8}T + 1.656\,10^{-10}T^2 \tag{5.69}$$

where D_w^k is the water Knudsen diffusion; D°_w, the water air diffusion; T, the temperature along the membrane; p_a is the partial pressure of air in the pore (it is assumed $p_a = 101{,}325$ Pa); τ, the tortuosity of the membrane; $\in$, the porosity of the membrane; δ, the thickness of the membrane; and r_p, the radius of the pores.

In membrane distillation, a temperature gradient is part of the driving force of the system. Thus the heat transfer coefficients in the feed (h_f) and permeate (h_p) (W m^{-2} K^{-1}) and the temperature polarization coefficient (TPC) can be calculated

from correlations (Gryta et al., 1997; Tun et al., 2005; Alkhudhiri et al., 2012; Lawson and Lloyd, 1997):

$$h = \frac{Nu\, k_{fluid}}{d} \tag{5.70}$$

$$Nu = 1.86\left(Re\, Pr \frac{d}{l}\right)^{0.33}\left(\frac{\eta}{\eta_w}\right)^{0.14} \tag{5.71}$$

$$\mathrm{Pr} = \frac{C_p \eta}{k_{fluid}} \tag{5.72}$$

where Nu and Pr are the Nusselt and Prandtl numbers, respectively; k_{fluid} is the thermal conductivity of the fluid ($\mathrm{W\,m^{-1}\,K^{-1}}$); d (m) is d_i and d_h for the feed and the osmotic side, respectively; η and η_w are the viscosity of the solution (feed or osmotic solution) and the water, respectively; C_p is the heat capacity ($\mathrm{J\,kg^{-1}\,K^{-1}}$); and k_{fluid} is the thermal conductivity of the fluid ($\mathrm{W\,m^{-1}\,K^{-1}}$).

The heat transfer through the membrane by conduction (h_c) and vapor movement (h_v), and the temperature polarization coefficient (TPC) are given by:

$$h_c = \frac{k_{mem}}{\delta} = \frac{\in k_g + (1-\in)k_s}{\delta} \tag{5.73}$$

$$h_v = \frac{J_w\, \Delta H_v}{\Delta T_w} \tag{5.74}$$

$$\Delta T_w = T_{fw} - T_{pw} \tag{5.75}$$

$$T_{fw} = T_f - \left(T_f - T_p\right)\left(\frac{\frac{1}{h_f}}{\frac{1}{h_c + h_v} + \frac{1}{h_f} + \frac{1}{h_p}}\right) \tag{5.76}$$

$$T_{pw} = T_p + \left(T_f - T_p\right)\left(\frac{\frac{1}{h_p}}{\frac{1}{h_c + h_v} + \frac{1}{h_f} + \frac{1}{h_p}}\right) \tag{5.77}$$

$$TPC = \frac{\Delta T_w}{T_f - T_p} \tag{5.78}$$

where k_{mem}, k_g, k_s are the thermal conductivity of the membrane, the air and the solid phase of the membrane, respectively; ΔH_v is the latent heat of vaporization ($\mathrm{J\,kg^{-1}}$); ΔT_w is the temperature difference (K) among the temperature near the membrane wall in the feed (T_{fw}) and the permeate side (T_{pw}).

The effect of the operating conditions such as the concentration of the osmotic solution, the feed concentration, and the temperature on the overall mass transfer coefficient gives very valuable information on possible effects of concentration or temperature polarization. On the other hand, studying the effect of the flow rates of the feed and osmotic solutions allows determining the degree of turbulence needed in the fluid phases to minimize their mass transfer resistance. Fig. 5.16 is an example of this kind of studies for the concentration and further crystallization of Na_2CO_3 using an osmotic solution of NaCl (Ruiz-Salmón and Luis, 2018). Flow rates under $50\,mL\,min^{-1}$ showed low turbulence, leading to concentration polarization. High concentration in the osmotic solution led to higher fluxes but the overall membrane coefficient did not increase as expected. A possible phenomenon of concentration polarization and/or membrane wetting could explain this loss of performance. In addition, increasing the temperature did not produce a significant increase of the overall mass transfer coefficient in spite of increasing the flux. Thus temperature polarization was observed. Regarding the heat transfer coefficient (Fig. 5.17), high concentration of the NaCl solution influences slightly the heat transfer but this effect disappears as soon as the feed temperature was increased above 35°C.

5.6 MEMBRANE EMULSIFICATION

Emulsions are mixtures consisting of a dispersed phase uniformly distributed in a continuous phase. Oil-in-water (o/w) emulsions have oil droplets uniformly dispersed in water. On the other hand, water-in-oil (w/o) emulsions present water droplets uniformly dispersed in oil. Systems with an emulsion as the dispersed phase are called multiple emulsions, like water-in-oil-in-water (w/o/w) emulsions. Emulsions play a critical role in the formulation of pharmaceutical compounds, cosmetics, food, pigment dispersions, and synthesis of latex. They are present in our daily life as creams, mayonnaise, butter, margarine, sauces, and so on. The conventional equipment used to prepare emulsions is typically based on colloid mills, high-speed rotor-stator systems, and high-pressure dispersing homogenizers. These methods achieve the desired size distribution of the droplets by the generation of turbulent breakup, where high shear stress is applied to deform and disrupt larger droplets in order to keep the stability of the emulsion and avoid coalescence. Energy consumption is generally elevated because only a fraction of the energy input is used for droplet breakup. In a high-pressure homogenizer about 99.8% of the energy supplied is lost and converted into heat (Drioli et al., 2005). Using a membrane contactor offers the advantage of decreasing energy consumption and achieving a homogenous size distribution of droplets. The working principle is different than with other systems using membrane contactors since in membrane emulsification, the dispersed phase is pressed through the membrane pores to the other side of the membrane. If a crossflow configuration is used, the droplets formed at the pore mouth are detached by the action of the drag force given by the tangential flow of the continuous phase flowing along the membrane surface (Giorno et al., 2005). Fig. 5.18 shows the working

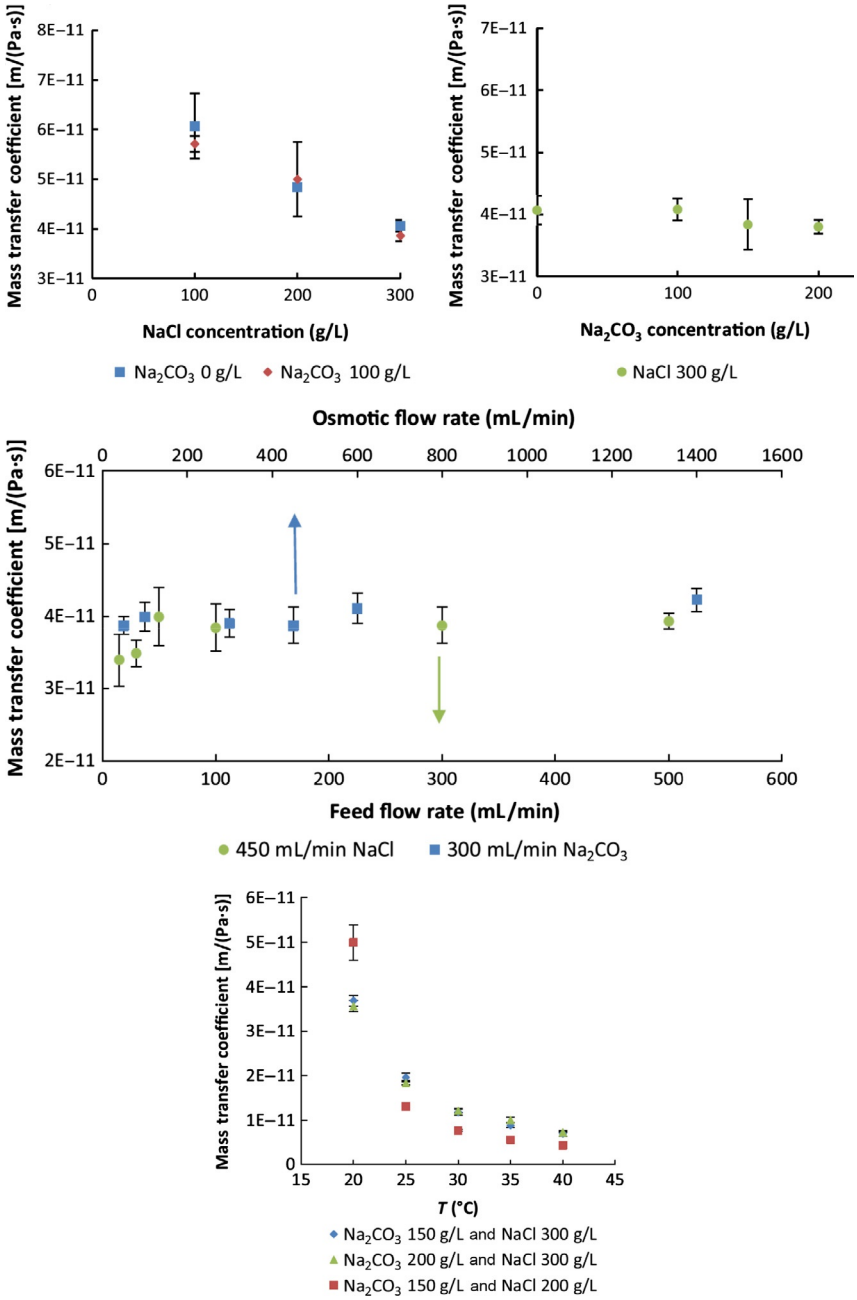

FIG. 5.16

Mass transfer coefficient as a function of (A) the concentration of Na_2CO_3 (feed solution); (B) the concentration of NaCl (osmotic solution); (C) the feed and osmotic flow rates (Na_2CO_3 and NaCl concentration are 150 and 300 $g\,L^{-1}$, respectively); (D) feed temperature.

Reproduced with permission from Ruiz-Salmón, I., Luis, P., 2018. Membrane crystallization via membrane distillation. Chem. Eng. Process. Process Intensif. 123, 258–271.

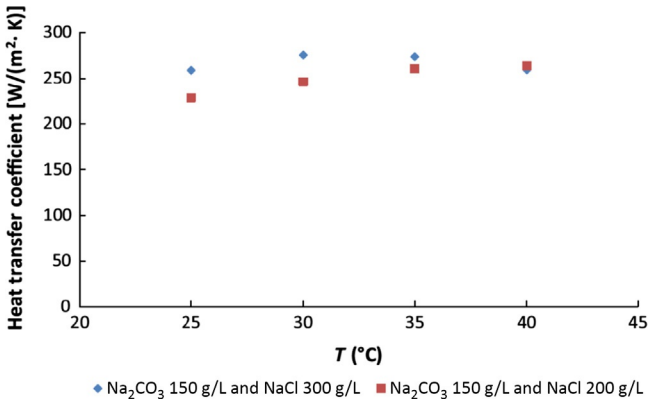

FIG. 5.17

Heat transfer coefficient as a function of the temperature.

Reproduced with permission from Ruiz-Salmón, I., Luis, P., 2018. Membrane crystallization via membrane distillation. Chem. Eng. Process. Process Intensif. 123, 258–271.

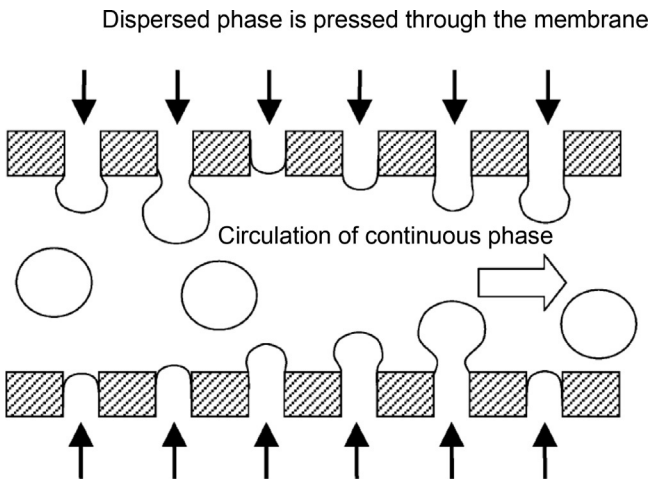

FIG. 5.18

Principle of membrane emulsification.

Reproduced with permission from Rayner, M., Tragardh, G., Tragardh, C., 2005. The impact of mass transfer and interfacial expansion rate on droplet size in membrane emulsification processes. Colloids Surf. A: Physicochem. Eng. Asp. 266, 1–17.

principle of membrane emulsification and Fig. 5.19 presents an example of emulsions created by using this technology.

A typical lab-scale system to perform experimental tests of membrane emulsification is shown in Fig. 5.20. The membrane contactor is the core of the experimental plant. A careful control of pressure and temperature is required. The permeate flux

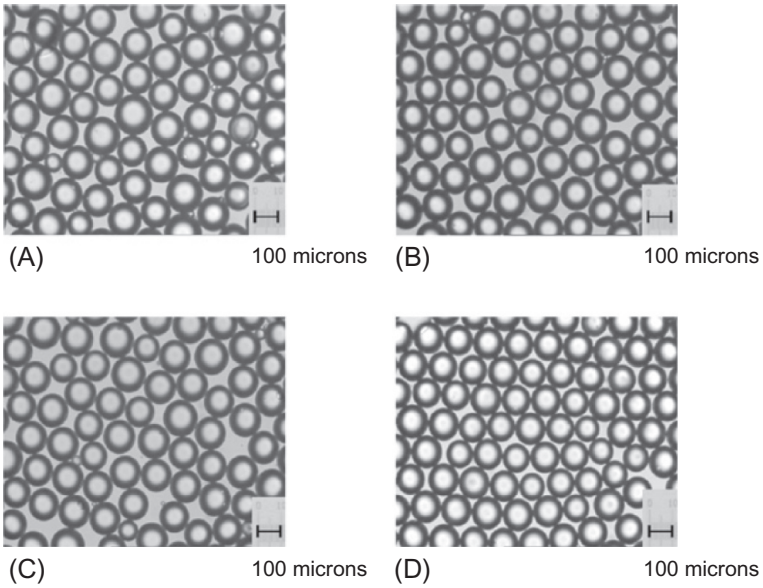

FIG. 5.19

Optical microscope images of drops formed using membranes with 80-μm pore spacing under different conditions: (A) 2 V agitation (3.5 Hz (210 rpm))—0.5 Pa peak shear at membrane; (B) 3 V agitation (5.6 Hz (340 rpm)—1.2 Pa peak shear at membrane; (C) 4 V agitation (6.833 Hz (410 rpm))—1.7 Pa peak shear at membrane; (D) 6 V agitation (10.833 Hz (650 rpm))—3.6 Pa peak shear at membrane.

Reproduced with permission from Egidi, E., Gasparini, G., Holdich, R.G., Vladisavljevic, G.T., Kosvintsev, S.R., 2008. Membrane emulsification using membranes of regular pore spacing: droplet size and uniformity in the presence of surface shear. J. Membr. Sci. 323, 414–420.

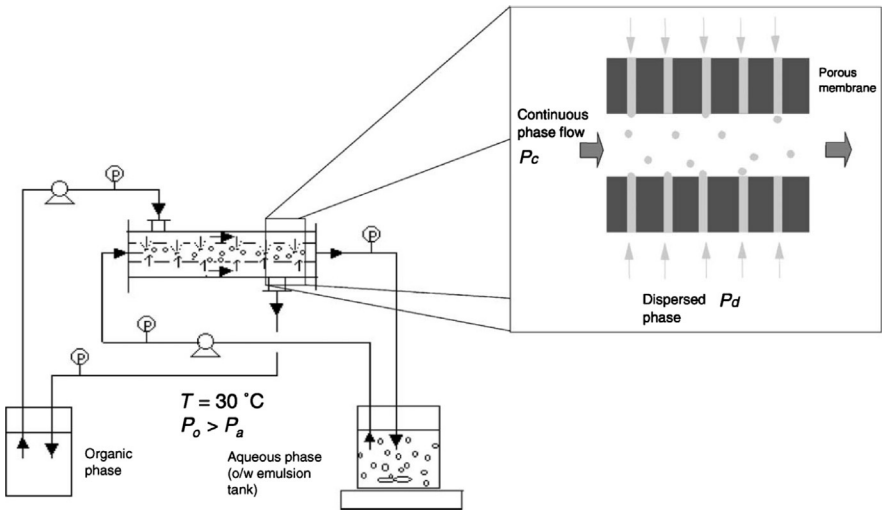

FIG. 5.20

Schematic representation of the membrane emulsification system.

Reproduced with permission from Giorno, L., Li, N., Drioli, E., 2003a. Preparation of oil-in-water emulsions using polyamide 10 kDa hollow fiber membrane. J. Membr. Sci. 217, 173–180, Giorno, L., Li, N., Drioli, E., 2003b. Use of stable emulsion to improve stability, activity, and enantioselectivity of lipase immobilized in a membrane reactor. Biotechnol. Bioeng. 84, 677–685.

(flux of the dispersed phase), J_d, can be calculated indirectly by measuring the weight decrease of the dispersed phase (Δw) as a function of time:

$$J_d = \frac{\Delta w}{\Delta t \cdot A} \tag{5.79}$$

where A is the membrane area.

The driving force is given by the transmembrane pressure, that is, the pressure difference between the dispersion phase and the continuous phase. Taking into account the pressure drop of the membrane contactor, the transmembrane pressure, ΔP_{TM}, can be calculated considering an average pressure between the inlet and the outlet of the contactor (Giorno et al., 2003a, b):

$$\Delta P_{TM} = \frac{1}{2}(P_{d,in} + P_{d,out}) - \frac{1}{2}(P_{c,in} + P_{c,out}) \tag{5.80}$$

where $P_{d,in}$ and $P_{d,out}$ are the pressure of the dispersion phase at the inlet and outlet, respectively, and $P_{c,in}$ and $P_{c,out}$ are the pressure of the continuous phase at the inlet and outlet, respectively. This transmembrane pressure should be higher than the breakthrough pressure indicated in Eq. (5.1) in order to press the dispersed fluid through the pores of the membrane.

The stability of the emulsions depends on several factors, such as the droplet size, the emulsifying agent, net charge, and mechanical and physical properties of the adsorbed film. Among these factors, the droplet size is the most important parameter. Microemulsions, or emulsions with droplet size in the range 20–80 nm, are thermodynamically stable mixtures of oil in water or water in oil. When droplets are larger, the interface between the oil and the water phase must be stabilized by surfactant molecules, which prevent immediate aggregation or coalescence and whose properties largely determine the behavior of the emulsion (Giorno et al., 2005). The final droplet size and size distribution are determined by the membrane material, pore size and porosity, as well as process parameters such as the crossflow velocity of the continuous phase and the transmembrane pressure.

The membrane material should be selected so that the membrane is not wetted with the dispersed phase. The reason behind this is that using hydrophobic membranes for making an o/w emulsion resulted in polydispersed emulsions with a larger average droplet size than when using a hydrophilic membrane (Nakashima et al., 1991). Making w/o emulsions using hydrophilic membranes has resulted in droplets smaller than the pore size and dependent on the structure of the pore and not only on the diameter (Kandori et al., 1991). Thus in oil-in-water emulsions (oil: dispersed phase; water: continuous phase), the membrane will be hydrophilic, whereas in water-in-oil emulsions (water: dispersed phase; oil: continuous phase), the membrane will be hydrophobic (Drioli et al., 2005). A typical membrane material in membrane emulsification is porous glass due to the widely used Shirasu porous glass (SPG) membrane (Ise Chemical *Co*, Japan) synthesized from CaO-Al_2O_3-B_2O_3-SiO_2-type glass made from "Shirasu," a Japanese volcanic ash (Nakashima et al., 1991). Other membranes have been used to prepare oil-in-water emulsions (commercial microfiltration membranes of ceramic α-alumina from Membraflow, Germany; α-alumina- and zirconia coated membranes from SCT, France;

polytetrafluoroethylene membranes from Advantec Tokyo Ltd. and Goretex, Japan) (Suzuki et al., 1998; Schröder and Schubert, 1999a,b; Joscelyne and Trägårdh, 1999; Kanichi et al., 2002; Yamazaki et al., 2002) or water-in-oil emulsions (microporous polypropylene hollow fibers from Microdyn, Germany; polytetrafluoroethylene membranes from Advantec, Japan) (Suzuki et al., 1998; Vladisavljevic et al., 2002). In order to achieve permeation of the organic phase when using hydrophilic membranes, or permeation of the aqueous phase through the hydrophobic membrane, a pretreatment of the membrane is thus necessary. This pretreatment normally consists on removing the internal liquid phase and substituting it by the phase to be dispersed. It may affect the pore size of the membranes, thus it is important to apply an appropriate pretreatment method in order to obtain the desired size of the droplets. Giorno et al. (2005) evaluated the effect of four different procedures on the final size of the droplets. Basically, the pretreatment consisted in washing the membrane with a gradient of miscible solvents and solvent solutions of decreasing polarity, to shift the internal phase from polar to nonpolar and to allow the permeation of the organic phase (Giorno et al., 2003a,b, 2005). Fig. 5.21 clearly shows the significant variation of the final droplet size depending on the pretreatment used due to the modification

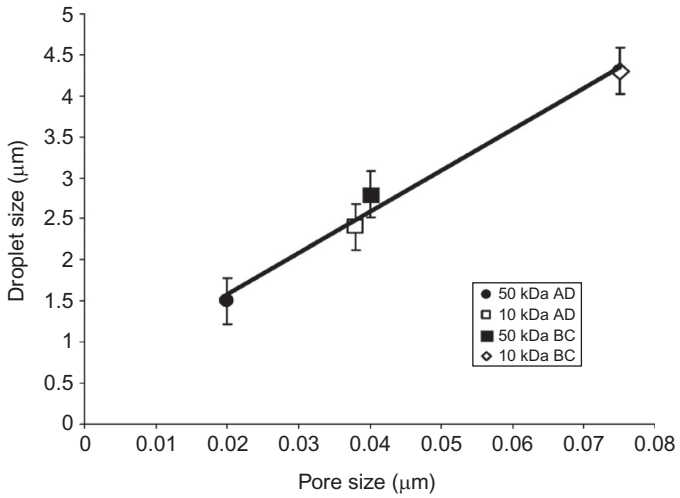

FIG. 5.21

Relationship between pore size and droplet size obtained by Giorno et al. (2005) using two membranes (polyamide capillary membranes with nominal molecular weight cutoff of 10 and 50 kDa) after pretreatment following four different procedures (A: subsequent permeation of pure water, water-isopropanol (50:50), and pure isooctane; B and C: pure water, water-isopropanol (80:20), isopropanol-isooctane (50:50 and 20:80), and then pure isooctane; the difference between B and C is the different contact time of membranes with the solutions; D: water, isopropanol-isooctane (50:50), and then pure isooctane).

Reproduced with permission from Giorno, L., Mazzei, R., Orioloa, M., De Luca, G., Davoli, M., Drioli, E., 2005. Effects of organic solvents on ultrafiltration polyamide membranes for the preparation of oil-in-water emulsions. J. Colloid Interface Sci. 287, 612–623.

of the membrane pore size. The effect of solvents on the thin layer of asymmetric polyamide membranes showed a clear change in the membrane morphology and pore structure.

Regarding the pore size, a linear correlation ($y = m\ x$) between membrane pore size (y) and droplet size (x) has been generally observed where the value of m may range from 2 to 10 depending on the properties of the organic, water, and membrane (Rayner and Tragardh, 2002). This effect can be also observed in Fig. 5.21. For SPG membranes, values of m range typically from 2 to 10. For membranes other than SPG, the values reported for m are higher, typically 3–50 (Charcosset et al., 2004).

Finally, the porosity of the membrane surface also plays an important role in the droplet size since it determines the distance between two adjacent pores, which is critical to ensure that two adjacent droplets do not come too close, leading to coalescence (Charcosset et al., 2004). As a reference, a maximum membrane porosity to prevent coalescence of droplets growing on neighboring pores of 5 μm diameter has found to be 1.5% (Abrahamse et al., 2001).

Process parameters influence the final size and distribution of droplets in the emulsion as well. The crossflow velocity will cause the detachment of droplets formed at the membrane surface. The droplet size becomes smaller as the wall shear stress (caused by the crossflow of the continuous phase) increases (Charcosset et al., 2004). Fig. 5.22 shows the variation of droplet diameter observed by Rayner and Tragardh (2002) as a function of the wall shear stress. An appropriate control of the flow rate of the continuous phase is thus essential.

Another process parameter is the transmembrane pressure. Increasing the transmembrane pressure will increase the flux of the dispersed phase through the

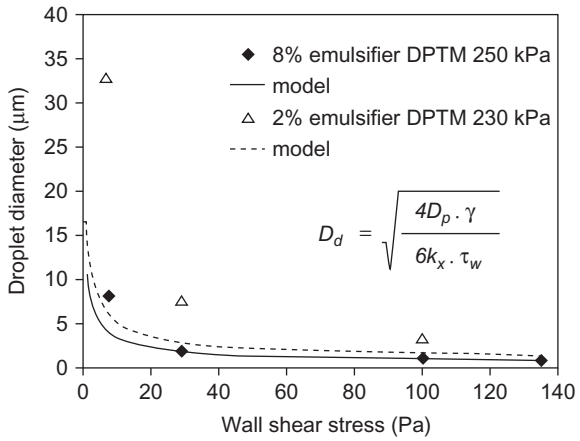

FIG. 5.22

Variation of droplet diameter with the wall shear stress.

Reproduced with permission from Rayner, M., Tragardh, G., 2002. Membrane emulsification modelling: how can we get from characterization to design? Desalination 145, 165–172.

membrane according to the Darcy's law, but it will also increase the average droplet pore size and the size distribution because of droplet coalescence at the membrane surface. Fig. 5.23 shows an example of the effect of the transmembrane pressure on the flux of the dispersed phase. Adding surfactants may become a need to have high transmembrane flux while keeping the formation of small droplets.

The mathematical description of the mass transfer in membrane emulsification begins with the application of Darcy's law, which relates the dispersed phase flux, J_d, to the transmembrane pressure, AP_{TM}:

$$J_d = \frac{\beta \cdot \Delta P_{TM}}{\mu\delta} \tag{5.81}$$

where β is a factor, which can be called permeability, that depends on the membrane structure, δ is the membrane thickness, and μ is the viscosity of the dispersed phase (Rayner and Tragardh, 2002; Charcosset et al., 2004). If the membrane is assumed to have n uniform cylindrical pores of radius r, the permeability β can be calculated from the Hagen-Poiseuille equation (Charcosset et al., 2004):

$$\beta = \frac{nr^2}{8\pi} \tag{5.82}$$

Using an overall mass transfer coefficient, $K_{overall}$, defined as $K_{overall} = \frac{\beta}{\mu\delta}$ is also useful when studying membrane emulsification, and the application of the resistance-in-series model could be of interest to determine the main mass transfer limitations.

A limiting factor for emulsion production on a commercial scale is the low flux of the disperse phase through the membrane. Thus achieving a good mass transfer

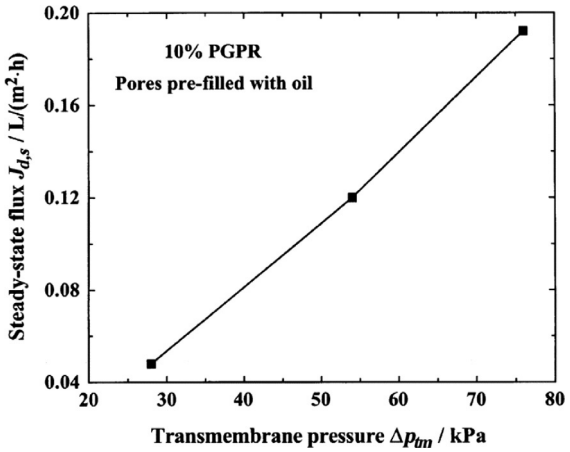

FIG. 5.23

Steady-state dispersed phase flux versus transmembrane pressure through the pores.
Reproduced with permission from Vladisavljevic, G.T., Tesch, S., Schubert, H., 2002. Preparation of water-in-oil emulsions using microporous polypropylene hollow fibers: influence of some operating parameters on droplet size distribution. Chem. Eng. Process. 41, 231–238.

through the membrane is a key objective in current research. The porosity and pore size of the membrane will influence the mass transport as well as the mass transfer resistance produced by the liquid phases. In order to decrease the mass transfer resistance produced by the liquid phases, an appropriate control of the fluid dynamics is required (Joscelyne and Trägårdh, 2000). Controlling the droplet size is also crucial in the emulsification process. It involves having a deep knowledge about the process of droplet formation and detachment at the membrane surface, the behavior of the dispersed phase through the membrane itself, and other phenomena that may occur within the process (Vladisavljeviæ and Schubert, 2003). Research on modeling of membrane emulsification is thus oriented to develop mathematical models that predict the effect of input parameters (e.g., transmembrane pressure, shear rate, membrane pore size) on process output (e.g., droplet size, production rate) (Spyropoulos et al., 2014). In this way, a good control over the final properties of the emulsion can be achieved.

If emulsifiers (substances that confer long-term stability) or surfactants (surface active agents that reduce interfacial tension) are added into the emulsion, the droplet size will be modified due to their coupled transport to the expansion rate of the oil-water interface. The type of surfactant used influences significantly the droplet size (Schröder et al., 1998; Schröder and Schubert, 1999a, b). The viscosity of the dispersed phase has an important effect on the transmembrane flux and the droplet size. If the viscosity of the dispersed phase is high, the flux through the membrane will be low (see equation X-Darcy), and as a consequence, the droplet diameter will be large compared with the mean pore diameter (Charcosset et al., 2004).

Droplet expansion and adsorption at the interface are coupled, thus the rates of droplet expansion and droplet detachment as well as the adsorption rate of the emulsifier/surfactant to the growing interfacial area become relevant over the involved time scales (Rayner et al., 2005). When a new droplet begins to grow from a pore, some surfactant is already present at the interface. However, the surfactant surface coverage decreases over time because the area of the droplet is increasing. The consequence is that additional surfactant molecules can be adsorbed, which leads to the transport of the surfactant to the surface droplet. In order to obtain the surface coverage of the emulsifier/surfactant over time, the mass transfer coefficient in the continuous phase, k_{cts}, should be analyzed. Two cases can be considered (Rayner et al., 2005):

Case i: low wall shear rates where the process is dominated by molecular diffusion through an "infinite" boundary layer. In this case, it is observed that

$$\pi \leq \frac{\partial^2}{Dt} < \infty \tag{5.83}$$

where D is the diffusion coefficient of the surfactant, δ is the boundary layer height, and t is the droplet formation time.

The penetration theory is then applied to calculate the point value of the mass transfer coefficient in the continuous phase:

$$k_{cts} = \sqrt{\frac{D}{\pi t}} \tag{5.84}$$

The penetration theory (Higbie, 1935) considers that the depth of penetration is less than the total depth of the liquid boundary layer, thus the total depth is assumed to be infinite. Velocity gradients within the fluids are ignored since mass transport takes place mainly by molecular diffusion and a balance for the surfactant in the continuous phase is governed by Fick's second law.

Case ii: moderate wall shear rates where both diffusion and flow convection are taken into account. In this case:

$$\frac{\partial^2}{Dt} < \pi \tag{5.85}$$

The Reynolds analogy is applied to calculate the mass transfer coefficient:

$$k_{cts} = \frac{\tau_{wall}}{\rho U} \frac{1}{1 + \alpha(Sc - 1)} \tag{5.86}$$

where U is the average velocity in the continuous phase; ρ is the density; τ_{wall} is the wall shear stress; α is the ratio of the velocity at the edge of the viscous sublayer to the average velocity (equal to 2.0 $Re^{-1/8}$ for pipe flow); and the Schmidt number, Sc, gives the dimensionless relationship. The Reynolds analogy relates the heat and mass transfer rates to momentum transfer through shear stress. It assumes that elements of fluid are brought from remote regions in the bulk to the surface by the action of turbulent eddies without mixing with the intermediate fluid along the way, and instantaneously reach equilibrium upon contact with the interfacial layers (Coulson and Richardson, 1999). This theory has been extended for viscous sublayers by Taylor and Prandlt (Taylor, 1916; Prandlt, 1910, 1928).

The diffusion coefficient of the polymeric surfactant, D, can be calculated by the Stokes-Einstein equation:

$$D = \frac{kT}{a\mu} \tag{5.87}$$

where k is the Boltzmann constant, T is temperature, μ is viscosity of the continuous phase, and a is the length of the molecule which is assumed to be two times the radius of gyration of a polymer in solution ($R_g \approx M_W^{0,6} x 10^{-9}$ nm).

The reader is addressed to Rayner et al. (2005) for a complete mathematical description of the transport process indicated in cases *i* and *ii*.

Modeling the droplet size as a function of the kind of mechanism that will cause the detachment of the droplets from the membrane surface (produced spontaneously or due to shear stress) has been performed intensively in the literature (Yasuno et al., 2002; Kobayashi et al., 2003; Christov et al., 2002; Sugiura et al., 2001; Rayner et al., 2004; Schröder and Schubert, 1999a, b; Joscelyne and Trägårdh, 1999). Droplet formation spontaneously occurs when the droplet break off occurs due to the minimization of free energy (a crossflow is not applied) (Sugiura et al., 2001; Rayner et al., 2004). On the other hand, shear-induced droplet formation happens when the flow of a continuous phase produces a shear stress on the emerging droplets, causing their detachment from the surface. The continuous phase produces thus an effect on

the size and distribution of the droplets. In this case, the droplet diameter can be predicted based on a force balance, in which the capillary force and the opposing drag force seem to be the most important. Works performed by Rayner et al. (2004), Peng and Williams (1998), and Schröder et al. (1998) can be taken as an starting point for interested readers.

5.7 CONTACTOR MEMBRANE REACTORS

Membrane reactors combine reaction and a membrane process in the same single unit creating synergies. In general terms, there are three main systems that fit within the category of a membrane reactor: "extractor," "distributor," and "contactor" (Westermann and Melin, 2009). The "extractor" selectively removes the products from the reaction mixture; the "distributor" controls the addition of reactants to the reaction mixture; and the "contactor" intensifies the contact between reactants. In this chapter, the contactor concept will be considered.

In a contactor membrane reactor, the membrane can be used in two main ways (Fig. 5.24): (*i*) the membrane is a barrier between two fluid phases (gas-liquid or liquid-liquid phases) that will contact each other inside the pores of the membrane (interfacial contactor). The reaction takes place inside the pores and the reaction product will have preference by one or both phases. The membrane can be catalytically active or the catalyst can be in the feed solution. In the latter case, an extractant is required at the other side of the membrane with high selectivity for the reaction product; or (*ii*) the fluid phase containing the reagents is pushed through the membrane pores. In contact with catalyst, the reaction will take place and the reaction product will be collected at the other side of the membrane. In this case, the membrane is always catalytically active, thus the reaction will take place on the catalytic sites within the membrane structure.

(a) Interfacial contactor that separates two immiscible reagents. The catalyst is within the membrane pores:
(b) Interfacial contactor that uses an extractant to extract selectively the reaction product. The catalyst is within the membrane pores or in the feed fluid phase:
(c) Forced flow-through contactor in which the feed fluid phase goes through the membrane pores. The catalyst is within the membrane pores:

5.7.1 INTERFACIAL MEMBRANE CONTACTOR

In a gas-liquid configuration based on the interfacial contactor (Fig. 5.24A), the catalytically active layer faces the liquid side. The gas diffuses through the membrane support layer and dissolves in the liquid at the gas-liquid interface. This gas-liquid interface will be placed somewhere within the membrane pores depending on the transmembrane pressure. The reaction zone is located inside the catalytically active membrane, preferentially with partially wetted active sites, which consequently

Interfacial contactor that separates two immiscible reagents.

The catalyst is within the membrane pores:

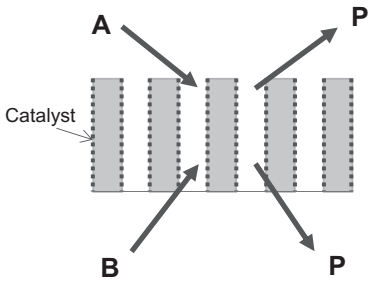

(A)

Interfacial contactor that uses an extractant to extract selectively the reaction product.

The catalyst is within the membrane pores or in the feed fluid phase:

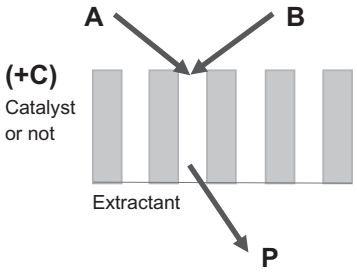

(B)

Forced-flow through contactor in which the feed fluid phase goes through the membrane pores.

The catalyst is within the membrane pores:

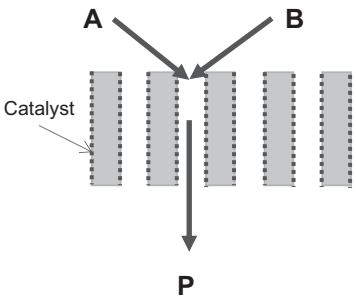

(C)

FIG. 5.24

Principles of contactor membrane reactors for the reaction A + B → P: (A) interfacial contactor separating two immiscible reagents; (B) interfacial contactor using an extracting agent, and (C) forced flow-through contactor.

increases the concentration of gaseous reactant on these sites and enhances the overall reaction rate (Vospernik et al., 2003). The solute further diffuses through the liquid-filled pores and reacts at the catalytically active sites that are located at the pore walls. The reaction products normally tend to diffuse in the direction of the liquid side due to the pressure gradient (Westermann and Melin, 2009). This kind of configuration allows a lot of operational freedom: the gas and liquid flow rates can be varied independently, the transmembrane pressure can be adapted to control the location of the gas-liquid interface, additional substances can be targeted to the catalytic region without mass transfer resistances, and low pressures can be applied since the gas is supplied directly where it is consumed. Some examples of this configuration can be found in the recent literature (Sanchez Marcano and Tsotsis, 2002).

In aqueous-organic contactor, the membrane contactor separates two immiscible phases (Fig. 5.24A and B). The porous membrane is not permselective, but it simply assures well-defined separation and contact between the two liquid phases flowing from opposite sides of the membrane. The membrane can be inert with the catalyst being dissolved in one of the fluid phases, or it can be catalytically active if the catalyst is deposited on the surface of the membrane in order to promote the reaction between adsorbed reactant species. The membrane defines the reaction volume by providing a contacting zone for two immiscible phases. As in the gas-liquid system, the use of membrane contactors introduces a large flexibility in the operation since the flow rates of the two phases involved can be changed independently, as well as the reactant concentration and pressures. A typical application is in phase transfer catalysis, where two immiscible phases containing a water soluble nucleophilic reagent and an organic soluble electrophilic reagent (e.g., anions and organic substrates) are contacted, and a phase transfer catalyst (usually salts like tetraalkylammonium and tetraalkylphosphonium) is used to transfer a reactant from one of these phases into the other, allowing the reaction to occur (Drioli et al., 2005). The separation of the product and the phase transfer catalyst is a main technical challenge where membrane technology (nanofiltration and membrane contactors) offers the possibility of a nondestructive separation that allows reusing the catalyst (DeSmet et al., 2001; Scarpello et al., 2002; Bono et al., 1997; Lopez and Matson, 1997; Noworyta, 2001; Trusek-Holownia and Noworyta, 2002; Giorno et al., 2003b). The microporous membrane used in membrane contactors contributes to increasing the extraction flux due to its large surface. The transfer of the reaction product from the aqueous media to the organic phase enables equilibrium-limited reactions to be carried out to completion due to the combination of catalytic and separation processes, such as in transesterification reactions (Maia Filho et al., 2016). The membrane material may have a hydrophobic or hydrophilic character, thus the membrane will belong to the organic or aqueous phase, respectively (Drioli et al., 2005). Fig. 5.25 shows the typical mechanism in phase transfer catalysis. There is ions partition between the two phases, and the reaction rate is determined by intrinsic kinetics and transport rate (Jia et al., 2014). In case of the presence of the extraction phase, the membrane allows for contact of the reaction medium with the extraction phase without emulsion formation or typical phase separation problems (Sirkar, 2008).

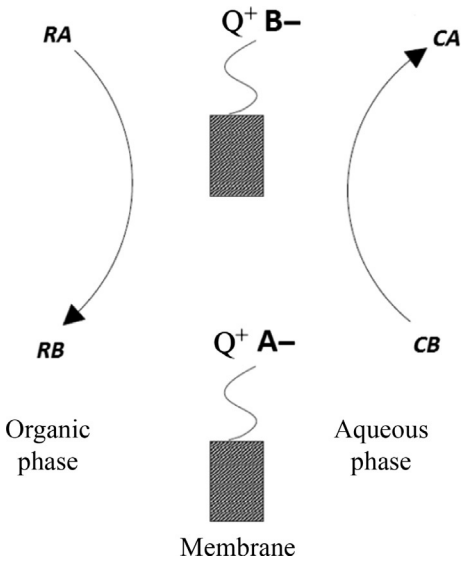

FIG. 5.25

Diagram of phase transfer catalysis mechanism.

Modified from Jia, Z., Zhen, T., Zhang, X., 2014. Application of phase-transfer catalytic membrane reactor in liquid–liquid nucleophilic substitution reaction: effects of operating parameters. J. Membr. Sci. 454, 316–321.

A typical experimental system using a contactor membrane reactor as an interfacial contactor is shown in Fig. 5.26 for liquid-liquid systems and gas-liquid systems. Hollow fiber membrane contactors are very common in this application due to their high membrane surface per unit of volume. However, other configurations based on flat membranes can be found in the literature (Maia Filho et al., 2016).

5.7.2 FORCED FLOW THROUGH

In interfacial membrane contactors, mass transport limitation by pore diffusion can occur if the reaction is very fast. A way to minimize the pore diffusion is to pump the whole reaction solution through an asymmetric (ceramic) membrane or a support coated with catalytically active metals (Reif and Dittmeyer, 2003). This configuration is called forced flow-through mode (Fig. 5.24C), where the reactants are premixed and supplied from the same side. The membrane is providing the reaction space with short controlled residence time and high catalytic activity. The objective is to reach complete conversion in minimum time or space, taking advantage of the high catalytic efficiency, or to reach maximum selectivity for a given reaction due to the narrow contact time distribution (Westermann and Melin, 2009). If the reaction solution is pumped through the membrane fast enough, there will not be concentration gradients in the pore system of the catalytic layer and pore diffusion can be totally eliminated. However, if the reaction is not fast enough to achieve a total

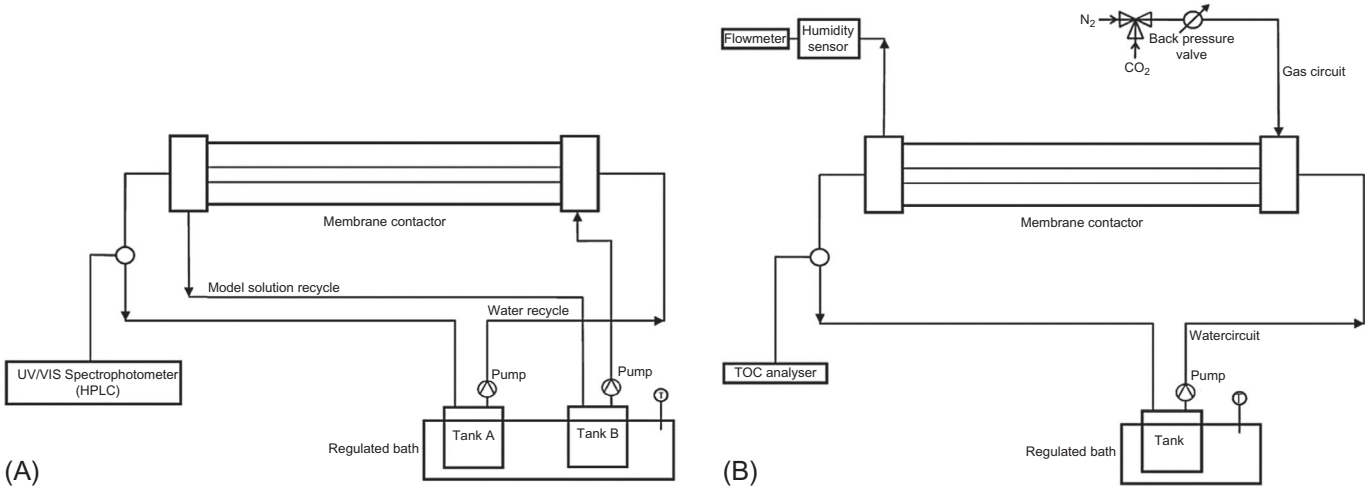

FIG. 5.26

Schematic drawing of a ceramic membrane contactor for (A) L-L and (B) G-L mass transfer studies.

Reproduced with permission from Vospernik, M., Pintar, A., Bercic, G., Levec, J., 2003. Mass transfer studies in gas–liquid–solid membrane contactors. Catal. Today 79–80, 169–179.

conversion with one pass through the membrane, a product recycle is necessary (Reif and Dittmeyer, 2003). In this configuration, gas-phase reaction (e.g., isomerization of 1-butene, CO oxidation, decomposition of VOCs) or liquid-phase reactions (e.g., water denitrification, sunflower oil partial hydrogenation) can take place.

In contactor membrane reactors, the study is normally focused on the reactor rate and the product yield and conversion. For example, considering the overall reaction:

$$\mathrm{RA\,(org) + CB\,(aq) \longleftrightarrow RB\,(org) + CA\,(aq)}$$

the apparent reaction rate can be calculated as (Jia et al., 2014):

$$-\frac{dC_{RA}}{dt} = k_{obs} C_{RA} C_{CB} \tag{5.88}$$

With k_{obs} the observed reaction rate constant, including the effects of intrinsic kinetics and mass transfer; C_{RBr} and C_{KI} are the concentration of RA and CB calculated using the whole volume (volume organic phase plus the volume of the aqueous phase) of the system. Solving the integral with $C_{CB}/C_{RA} = M$, and x as the conversion of RA at time t, leads to the following equation (Jia et al., 2014):

$$\frac{\ln(M-x)}{\ln(M(1-x))} \frac{}{C_{CB,0} - C_{RA,0}} = W = k_{obs} t \tag{5.89}$$

Thus plotting W versus t leads to a slope of value k_{obs}.

Several variables may affect the observed reaction rate constant, such as the concentrations and flow rates of the organic phase and the aqueous phase. Fig. 5.27 shows the effect of those variables on the reaction rate constant (slope) in an interface membrane reactor used for liquid-liquid nucleophilic reactions between *n*-bromooctane and KI aqueous solution, the overall reaction being RBr (org)+KI (aq) ↔ RI (org)+ KBr (aq) (Jia et al., 2014).

From those results, it is clear that mass transfer cannot be neglected in the interfacial membrane contactor. Varying the flow rate of the solutions has a large effect in the observed reaction rate constant, which is an indication of mass transfer resistance in the liquid phase. Diffusion is governing the mass transfer and limiting the reaction rate. In order to elevate the reaction rate, the flow rate of both phases should be increased. Increasing the concentration of the reagents lead also to an increase of the observed reaction rate constant, attributed to the increased diffusion rate of the ions Br^- and I^- from the organic phase and the aqueous phase, respectively, to the L-L interface. The structure and catalytic composition of the membranes presents also a relevant importance in the observed reaction rate constant (Jia et al., 2014). The selection of the appropriate pore dimensions strongly depends on the intended application and the allowable pressure drop (Westermann and Melin, 2009). Thus general guidelines or optimal work conditions are difficult to be established for the moment.

Due to the mass transfer limitations in interfacial membrane contactors, the forced-flow through contactor offers an interesting alternative that minimize diffusional problems. Reif and Dittmeyer (2003) presented the comparison of both

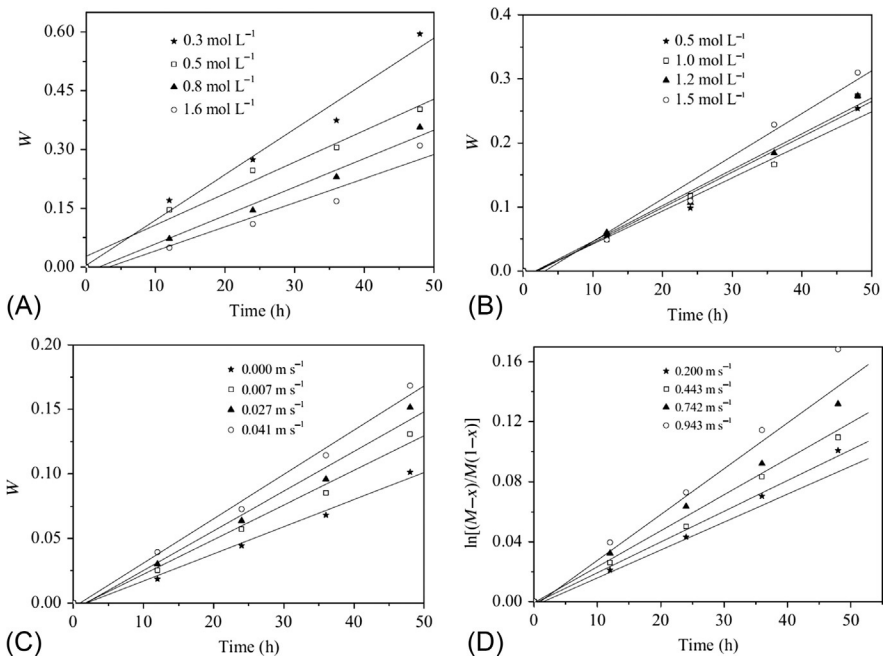

FIG. 5.27

Effects of (A) *n*-bromooctane concentration; (B) KI concentration; (C) KI flow rate; and (D) organic solution flow rate, on the observed reaction rate (slope) according to Eq. (5.89).

Reproduced with permission from Jia, Z., Zhen, T., Zhang, X., 2014. Application of phase-transfer catalytic membrane reactor in liquid–liquid nucleophilic substitution reaction: effects of operating parameters. J. Membr. Sci. 454, 316–321.

configurations to perform the catalytic nitrate/nitrite reduction in water. The reactions involved were as follows:

$$NO_3^- + H_2 \rightarrow NO_2^- + H_2O$$

$$2NO_2^- + 3H_2 \rightarrow N_2 + 2OH^- + 2H_2O \,(\text{desired})$$

$$2NO_2^- + 6H_2 \rightarrow 2NH_4^+ + 4OH^- \,(\text{undesired})$$

Fig. 5.28 shows the forced-flow through performance at different flow rates through the membrane in comparison with the interfacial contactor (catalytic diffuser) for catalytic nitrite reduction. The catalyst activity is not high when low flow rates are applied in the forced-flow contactor. The higher the flow rate through the membrane, the higher the catalyst activity until reaching a plateau value. The ammonium formation, which is the product of the undesired reaction, is also affected by the flow rate. The shorter the contact time in the porous support, the less ammonium is

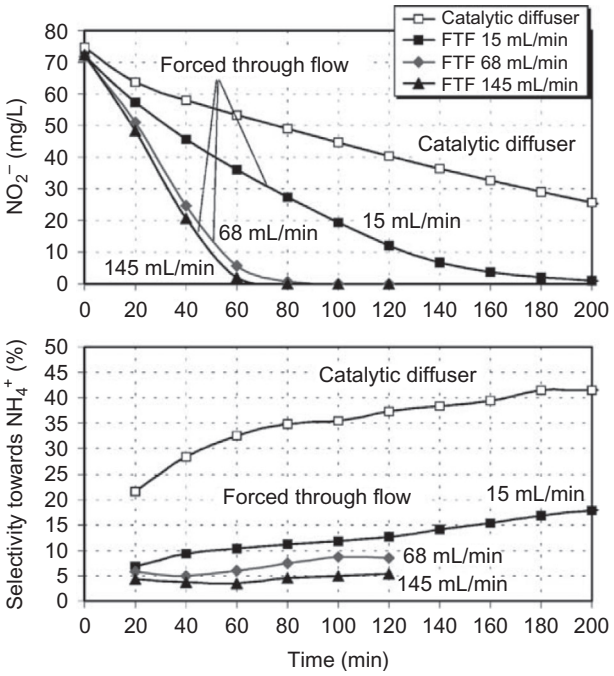

FIG. 5.28

Comparison between forced-flow through contactor at several flow rates through the membrane and interfacial contactor (catalytic diffuser). For the forced flow-through experiment: ceramic support (α-Al_2O_3); average pore diameter of 3 μm coated with 18.6 mg Pd. Water was externally saturated with gas (H_2:CO_2-ratio = 3:2) at atmospheric pressure. For the catalytic diffuser: asymmetric, tubular, ceramic membrane with a ZrO_2-top membrane layer with 18.6 mg Pd; 5 bar overpressure in membrane. H_2:CO_2-ratio = 3:2. Temperature: 20°C. Reaction volume in both experiments: 750 mL.

Reproduced with permission from Reif, M., Dittmeyer, R., 2003. Porous, catalytically active ceramic membranes for gas–liquid reactions: a comparison between catalytic diffuser and forced through flow concept. Catal. Today 82, 3–14.

produced. The interfacial contactor (catalytic diffuser) is presented as a less interesting option in terms of catalytic activity (Reif and Dittmeyer, 2003). The forced-flow contactor decreases the mass transport limitations and intensifies the contact between reactants and the catalytic material. However, membrane blocking and a higher energy consumption to push the fluid through the membrane are weak points of this configuration. Depending on the application, the interfacial contactor may be more advantageous. Conversion, mass transfer limitations, energy consumption, and blocking of the membrane are aspects that will affect directly the overall cost of the process and should be considered for a specific application.

REFERENCES

Abrahamse, A.J., van der Padt, A., Boom, R.M., Heij, W.B.C., 2001. Process fundamentals of membrane emulsification: simulation with CFD. AICHE J. 47, 1285–1291.

Alkhudhiri, A., Darwish, N., Hilal, N., 2012. Membrane distillation: a comprehensive review. Desalination 287, 2–18.

Bird, R.B., Stewart, W.E., Lightfoot, E.N., 2002. Transport Phenomena, second ed. Jonh Wiley & Sons, Inc., New York.

Bono, Y., Fukushima, K., Araya, G., Nabetani, H., Nakajima, M., 1997. Performance of perstractive enzyme reactor for synthesis of aspartame precursor. J. Chem. Technol. Biotechnol. 70, 171–178.

Charcosset, C., Limayem, I., Fessi, H., 2004. The membrane emulsification process—a review. J. Chem. Technol. Biotechnol. 79, 209–218.

Christov, N.C., Ganchev, D.N., Vassileva, N.D., Denkov, N.D., Danov, K.D., Kralchevsky, P.A., 2002. Colloids Surf. A Physicochem. Eng. Asp. 209, 83.

Coelhoso, I.M., Cardoso, M.M., Viegas, R.M.C., Crespo, J.P.S.G., 2000. Transport mechanisms and modelling in liquid membrane contactors. Sep. Purif. Technol. 19, 183–197.

Coulson, J.M., Richardson, J.F., 1999. Chemical Engineering, sixth ed. vol. 1. Butterworth Heinemann, Oxford.

Curcio, E., Drioli, E., 2005. Membrane distillation and related operations—a review. Sep. Purif. Rev. 34, 35–86.

Cussler, E.L., 1997. Diffusion. In: Mass Transfer in Fluid Systems, second ed. Cambridge University Press, United States of America.

DeSmet, K., Aerts, S., Ceulemans, E., Vankelecom, I.F.J., Jacobs, P.A., 2001. Nanofiltration-coupled catalysis to combine the advantages of homogeneous and heterogeneous catalysis. Chem. Commun. 597–598.

Drioli, E., Romano, M., 2001. Progress and new perspectives on integrated membrane operations for sustainable industrial growth. Ind. Eng. Chem. Res. 40, 1277–1300.

Drioli, E., Curcio, E., 2004. Perspectives for membrane contactors application in water treatment. J. Ind. Eng. Chem. 10 (1), 24–32.

Drioli, E., Curcio, E., Di Profio, G., 2005. State of the art and recent progresses in membrane contactors. Chem. Eng. Res. Des. J. 83, 223–233.

El-Naas, M.H., Al-Marzouqi, M., Marzouk, S.A., Abdullatif, N., 2010. Evaluation of the removal of CO_2 using membrane contactors: membrane wettability. J. Membr. Sci. 350, 410–416.

Faiz, R., Al-Marzouqi, M., 2009. Mathematical modeling for the simultaneous absorption of CO_2 and H_2S using MEA in hollow fiber membrane contactors. J. Membr. Sci. 342, 269–278.

Gabelman, A., Hwang, S., 1999. Hollow fiber membrane contactors. J. Membr. Sci. 159, 61–106.

Giorno, L., Na, L., Drioli, E., 2003a. Preparation of oil-in-water emulsions using polyamide 10 kDa hollow fiber membrane. J. Membr. Sci. 217, 173–180.

Giorno, L., Li, N., Drioli, E., 2003b. Use of stable emulsion to improve stability, activity, and enantioselectivity of lipase immobilized in a membrane reactor. Biotechnol. Bioeng. 84, 677–685.

Giorno, L., Mazzei, R., Orioloa, M., De Luca, G., Davoli, M., Drioli, E., 2005. Effects of organic solvents on ultrafiltration polyamide membranes for the preparation of oil-in-water emulsions. J. Colloid Interface Sci. 287, 612–623.

Gómez, E., González, B., Calvar, N., Tojo, E., Domínguez, A., 2006. Physical properties of pure 1-ethyl-3-methylimidazolium ethylsulfate and its binary mixtures with ethanol and water at several temperatures. J. Chem. Eng. Data 51, 2096–2102.

Gryta, M., 2005. Osmotic MD and other membrane distillation variants. J. Membr. Sci. 246, 145–156.

Gryta, M., Tomaszewska, M., Morawski, A.W., 1997. Membrane distillation with laminar flow. Sep. Purif. Technol. 11, 93–101.

Happel, J., 1959. Viscous flow relative to arrays of cylinders. AICHE J. 5, 174–177.

Higbie, R., 1935. The rate of absorption of a pure gas into a still liquid during short periods of exposure. Trans. Am. Inst. Chem. Eng. 31, 365–389.

Jia, Z., Zhen, T., Zhang, X., 2014. Application of phase-transfer catalytic membrane reactor in liquid–liquid nucleophilic substitution reaction: effects of operating parameters. J. Membr. Sci. 454, 316–321.

Joscelyne, S.M., Trägårdh, G., 2000. Membrane emulsification—a literature review. J. Membr. Sci. 169, 107–117.

Joscelyne, S.M., Trägårdh, G., 1999. Food emulsions using membrane emulsification: conditions for producing small droplets. J. Food Eng. 39, 59–64.

Kandori, K., Kishi, K., Ishikawa, T., 1991. Formation mechanisms of monodispersed W/O emulsions by SPG filter emulsification method. Colloids Surf. 61, 269–279.

Kanichi, S., Yuko, O., Yoshio, H., 2002. Properties of Solid Fat O/W Emulsions Prepared by Membrane Emulsification Method Combined with Pre-Emulsification.*3 i'eme Congr'es Mondial de l'Emulsion*, 24–27 September 2002, Lyon, France, p. 215.

Kobayashi, I., Nakajima, M., Mukataka, S., 2003. Colloids Surf. A Physicochem. Eng. Asp. 229, 33.

Lawson, K.W., Lloyd, D.R., 1997. Membrane distillation. J. Membr. Sci. 124, 1–25.

Li, W., Van der Bruggen, B., Luis, P., 2014. Integration of reverse osmosis and membrane crystallization for sodium sulphate recovery. Chem. Eng. Process. Process Intensif. 85, 57–68.

Li, W., Van der Bruggen, B., Luis, P., 2016. Recovery of Na_2CO_3 and Na_2SO_4 from mixed solutions by membrane crystallization. Chem. Eng. Res. Des. 106, 315–326.

Lopez, J., Matson, S., 1997. A multiphase/extractive enzyme membrane reactor for production of diltiazem chiral intermediate. J. Membr. Sci. 125, 189–211.

Lu, J., Wang, L., Sun, X., Li, J., Liu, X., 2005. Absorption of CO_2 into aqueous solutions of methyldiethanolamine and activated methyldiethanolamine from a gas mixture in a hollow fiber contactor. Ind. Eng. Chem. Res. 44, 9230–9238.

Lu, J., Zheng, Y.F., Cheng, M.D., 2008. Wetting mechanism in mass transfer process of hydrophobic membrane gas absorption. J. Membr. Sci. 308, 180–190.

Luis, P., Van der Bruggen, B., 2013. The role of membranes in postcombustion CO_2 capture. Greenhouse Gas Sci. Technol. 3, 1–20. https://doi.org/10.1002/ghg.

Luis, P., Garea, A., Irabien, A., 2010. Modelling of a hollow fiber ceramic contactor for SO_2 absorption. Sep. Purif. Technol. 72, 174–179.

Luis, P., Garea, A., Irabien, A., 2008. Sulfur dioxide non-dispersive absorption in N,N-dimethylaniline using a ceramic membrane contactor. J. Chem. Technol. Biotechnol. 83, 1570–1577.

Luis, P., Garea, A., Irabien, A., 2009. Zero solvent emission process for sulfur dioxide recovery using a membrane contactor and ionic liquids. J. Membr. Sci. 330, 80–89.

Luis, P., Van Aubel, D., Van der Bruggen, B., 2013. Technical viability and exergy analysis of membrane crystallization: closing the loop of CO_2 sequestration. Int. J. Greenhouse Gas Control 12, 450–459.

Maia Filho, D.C., Salim, V.M.M., Borges, C.P., 2016. Membrane contactor reactor for transesterification of triglycerides heterogeneously catalyzed. Chem. Eng. Process. 108, 220–225.
Nakashima, T., Shimizu, M., Kukizaki, M., 1991. Membrane emulsification by microporous glass. Key Eng. Mater. 61–62, 513–516.
Noworyta, A., 2001. Membrane reactors. In: Noworyta, A., Trusek-Holownia, A. (Eds.), Membrane Separations. Argi, Wroclaw, pp. 97–119.
Peng, S.J., Williams, R.A., 1998. Controlled production of emulsions using a crossflow membrane—Part I: droplet formation from a single pore. Trans. IChemE 76A, 894–901.
Prandlt, L., 1910. Eine Beziehung zwischen Wärmeaustausch und Strömungswiderstand der Flüssigkeiten. Physik Z. 11, 1027.
Prandlt, L., 1928. Bemerkung über den Wärmeübergang im Röhr. Physik Z. 29, 487.
Ranke, J., Stolte, S., Störmann, R., Aming, J., Jastorff, B., 2007. Design of sustainable chemical products—the example of ionic liquids. Chem. Rev. 107, 2183–2206.
Rayner, M., Trägårdh, G., Trägårdh, C., Dejmek, P., 2004. Using the surface evolver to model droplet formation processes in membrane emulsification. J. Colloid Interface Sci. 279, 175–185.
Rayner, M., Tragardh, G., Tragardh, C., 2005. The impact of mass transfer and interfacial expansion rate on droplet size in membrane emulsification processes. Colloids Surf. A: Physicochem. Eng. Asp. 266, 1–17.
Rayner, M., Tragardh, G., 2002. Membrane emulsification modelling: how can we get from characterization to design? Desalination 145, 165–172.
Raynie, D.E., 2006. Modern extraction techniques. Anal. Chem. 78, 3997–4003.
Reif, M., Dittmeyer, R., 2003. Porous, catalytically active ceramic membranes for gas–liquid reactions: a comparison between catalytic diffuser and forced through flow concept. Catal. Today 82, 3–14.
Ruiz-Salmón, I., Janssens, R., Luis, P., 2017. Mass and heat transfer study in osmotic membrane distillation-crystallization for CO_2 valorization as sodium carbonate. Sep. Purif. Technol. 176, 173–183.
Ruiz-Salmón, I., Luis, P., 2018. Membrane crystallization via membrane distillation. Chem. Eng. Process. Process Intensif. 123, 258–271.
Sandler, S.I., 2006. Chemical, Biochemical, and Engineering Thermodynamics, fourth ed. John Wiley & Sons, USA.
Sanchez Marcano, J.G., Tsotsis, T.T., 2002. Catalytic membranes and membrane reactors. Wiley-VCH, Weinheim.
San Román, M.F., Bringas, E., Ibañez, R., Ortiz, I., 2010. Liquid membrane technology: fundamentals and review of its applications. J. Chem. Technol. Biotechnol. 85, 2–10.
Scarpello, J.T., Nair, D., Freitas dos Santos, L.M., White, L.S., Livingston, A.G., 2002. The separation of organometallic catalysts using solvent resistant nanofiltration. J. Membr. Sci. 180, 1–15.
Schlosser, S., Sabolová, E., Kertész, R., Kubisová, L'., 2001. Factors influencing transport through liquid membranes and membrane-based solvent-extraction. J. Sep. Sci. 24, 509.
Schlosser, S., Kertész, R., Marták, J., 2005. Recovery and separation of organic acids by membrane-based solvent extraction and pertraction. An overview with a case study on recovery of MPCA. Sep. Purif. Technol. 41, 237–266.
Schröder, V., Behrend, O., Schubert, H., 1998. Effect of dynamic interfacial tension on the emulsification process using microporous, ceramic membranes. J. Colloid Interface Sci. 202, 334–340.

Schröder, V., Schubert, H., 1999a. Influence of emulsifier and pore size on membrane emulsification. Spec. Publ. R. Soc. Chem. 227, 70–80.
Schröder, V., Schubert, H., 1999b. Production of emulsions using microporous, ceramic membranes. Colloids Surf. A Physicochem. Eng. Asp. 152, 103–109.
Seader, J.D., Henley, E.J., Roper, K., 2011. Separation Process Principles: Chemical and Biochemical Operations, 3rd ed. Wiley, Hoboken, NJ.
Sengupta, A.; Peterson, P. A.; Miller, B. D.; Schneider, J.; Fulk, C. W., Jr. Large-scale application of membrane contactors for gas transfer from or to ultrapure water. Sep. Purif. Technol. 1998, 14, 189–200.
Sirkar, K.K., 2008. Membranes, phase interfaces, and separations: Novel techniques and membranes-an overview. Ind. Eng. Chem. Res. 47 (15), 5250–5266.
Sirkar, K.K., 1995. Membrane separations: newer concepts and applications for the food industry. In: Singh, R.K., Rizvi, S.S.H. (Eds.), Bioseparation Processes in Foods. Marcel Dekker, New York (Chapter 10).
Spyropoulos, F., Lloyd, D.M., Hancocks, R.D., Pawlik, A.K., 2014. Advances in membrane emulsification. Part B: recent developments in modelling and scale-up approaches. J. Sci. Food Agric. 94, 628–638.
Sugiura, S., Nakajima, M., Iwamoto, M., Seki, M., 2001. Interfacial tension driven monodispersed droplet formation from microfabricated channel array. Langmuir 17, 5562.
Suzuki, K., Fujiki, I., Hagura, Y., 1998. Preparation of corn oil/water and water/corn oil emulsions using PTFE membranes. Food Sci. Technol. 4, 164–167.
Taylor, G.I., 1916. Conditions at the Surface of a Body Exposed to the Wind. Brit. Adv. Com. Aero. Rep. Mem. No. 272, 423–429.
Trusek-Holownia, A., Noworyta, A., 2002. Catalytic membrane preparation for enzymatic hydrolysis reactions carried out in the membrane phase contactor. Desalination 144, 427–432.
Tun, C.M., Fane, A.G., Matheickal, J.T., Sheikholeslami, R., 2005. Membrane distillation crystallization of concentrated salts—flux and crystal formation. J. Membr. Sci. 257, 144–155.
Viegas, R.M.C., Rodríguez, M., Luque, S., Alvarez, J.R., Coelhoso, I.M., Crespo, J.P.S.G., 1998. Mass transfer correlations in membrane extraction: analysis of Wilson-plot methodology. J. Membr. Sci. 145, 129–142.
Vladisavljeviæ, G.T., Schubert, H., 2003. Influence of process parameters on droplet size distribution in SPG membrane emulsification and stability of prepared emulsion droplets. J. Membr. Sci. 225, 15–23.
Vladisavljevic, G.T., Tesch, S., Schubert, H., 2002. Preparation of water-in-oil emulsions using microporous polypropylene hollow fibers: influence of some operating parameters on droplet size distribution. Chem. Eng. Process. 41, 231–238.
Vospernik, M., Pintar, A., Bercic, G., Levec, J., 2003. Mass transfer studies in gas–liquid–solid membrane contactors. Catal. Today 79–80, 169–179.
Westermann, T., Melin, T., 2009. Flow-through catalytic membrane reactors—principles and applications. Chem. Eng. Process. 48, 17–28.
Yamazaki, N., Yuyama, H., Nagai, M., Ma, G.H., Omi, S., 2002. A comparison of membrane emulsification obtained using SPG (Shirasu porous glass) and PTFE [poly(tetrafluoroethylene)] membranes. J. Dispers. Sci. Technol. 23, 279–292.
Yang, D., Barbero, R.S., Devlin, D.J., Cussler, E.L., Colling, C.W., Carrera, M.E., 2006. Hollow fibers as structured packing for olefin/paraffin separations. J. Membr. Sci. 279, 61–69.

Yasuno, M., Nakajima, M., Iwamoto, S., Maruyama, T., Sugiura, S., Kobayashi, I., Shono, A., Satoh, K., 2002. Visualisation and characterization of SPG membrane emulsification. J. Membr. Sci. 210, 29.

Ye, W., Lin, J., Shen, J., Luis, P., Van der Bruggen, B., 2013. Membrane crystallization of sodium carbonate for carbon dioxide recovery: effect of impurities on the crystal morphology. Cryst. Growth Des. 13, 2362–2372.

Ye, W., Lin, J., Tækker Madsen, H., Gydesen Søgaard, E., Hélix-Nielsen, C., Luis, P., Van der Bruggen, B., 2016. Enhanced performance of a biomimetic membrane for Na_2CO_3 crystallization in the scenario of CO_2 capture. J. Membr. Sci. 498, 75–85.

Younas, M., Druon-Bocquet, S., Sanchez, J., 2011. Experimental and theoretical mass transfer transient analysis of copper extraction using hollow fiber membrane contactors. J. Membr. Sci. 382, 70–81.

FURTHER READING

Karoor, S., Sirkar, K., 1993. Gas absorption studies in microporous hollow fiber membrane modules. Ind. Eng. Chem. Res. 32, 674–684.

Zheng, J.M., Xu, Y.Y., Xu, Z.K., 2003. Shell side mass transfer characteristics in a parallel flow hollow fiber membrane module. Sep. Sci. Technol. 38, 1247–1267.